Is maximising current density always the optimum strategy in electrolyser design for electrochemical CO_2 conversion to chemicals?

Sahil Garg[a,1], Mengran Li [a,2,*], Mohamed Nazmi Idros [a], Yuming Wu [a], Geoff G.X. Wang [a], Thomas E. Rufford [a,*]

[a] *School of Chemical Engineering, the University of Queensland, St Lucia, 4072, Brisbane, Queensland, Australia*

[1] Present address for S. Garg: *Surface Physics and Catalysis (SurfCat) Section, Department of Physics, Technical University of Denmark, 2800 Kgs. Lyngby, Denmark*

[2] Present address for M. Li: *Materials for Energy Conversion and Storage (MECS), Department of Chemical Engineering, Faculty of Applied Sciences, Delft University of Technology, van der Maasweg 9, 2629 HZ Delft, The Netherlands*

**Corresponding authors: T.Rufford t.rufford@uq.edu.au; M. Li m.li6@uq.edu.au*

Abstract

Electrochemical conversion of CO_2 to chemicals and fuels can potentially play a role in reducing CO_2 emissions from industrial processes and providing non-fossil fuel routes to important chemical feedstocks. Most of the recent research on electrocatalysts for CO_2 reduction (CO_2R) focuses on achieving maximum selectivity for desired products at the highest possible current density. This approach assumes that maximising current density leads to the lowest cost of CO_2R (e.g. $\$\cdot kg^{-1}$ CO_2 converted) because it requires the lowest catalyst loadings and electrode area per kg of CO_2 treated and thus minimising the electrolyser equipment cost. Using a techno-economic analysis (TEA) model with experimental data from a two-cell vapor fed electrolyser, we show this assumption is not valid for CO_2 conversion to CO if the process model accounts for relationships between current density, selectivity, cell voltage, ohmic losses, and product separation costs. Instead, our model predicts the lowest CO production costs at current densities from 500 – 700 $A\cdot m^{-2}$. At current densities above 1000 $A\cdot m^{-2}$, growing ohmic losses in the electrolyser lead to increasing power costs that become much larger than any capital savings related to reduced electrode area at the higher current density. Further, we investigate different opportunities that could bring down the CO production cost, however, in all the cases, the lowest CO production cost was found at current densities between 600 – 1400 $A\cdot m^{-2}$. This work also provides insights that can help identify feasible design spaces for both catalysts and electrolysers to develop CO_2 conversion technologies that could soon compete on a cost basis with the natural reforming technologies to produce CO (0.60 $\$\cdot kg^{-1}$ market price).

1 Introduction

Electrochemical CO_2 reduction (CO_2R) powered by renewable energy sources is a promising technology to upgrade captured CO_2 from industrial waste gases into chemical feedstocks, such as carbon monoxide, ethylene, or formic acid.[1] This approach could help reduce emissions and decarbonise manufacturing industries like cement, iron and steel making, and food processing. Although electrochemical CO_2R technologies are in pilot-scale demonstrations, the cost of commercial CO_2 conversion to chemicals remains more expensive than the incumbent processes used to manufacture chemicals from petroleum-derived feedstocks.[2] Significant research efforts are being directed to developing highly selective and efficient CO_2R catalysts[3, 4], ion-exchange membranes[5], and electrolyzer configurations to improve performance and lower CO_2 conversion costs. In addition to these fundamental and engineering efforts, there is a need to improve the process and techno-economic models used to assess the potential economic feasibility of CO_2R technologies and identify feasible design spaces for new catalysts and electrolysers. Here, we report a new techno-economic model for CO_2R to CO validated with data from a lab-scale vapor-fed electrolyser and used this model to explore relationships between the operating current density and costs of CO production.

Several techno-economic analyses (TEA) reported in the literature – notably, studies by Jouny et al.[6], Spurgeon and Kumar[7], Verma et al.,[8] and De Luna et al.[9] – provide insights into the overall CO_2R process to highlight the future potential of electrochemical CO_2R technologies and critical challenges. For example, based on available technologies in current market environments, these studies concluded that carbon monoxide (CO) and formic acid/formate production are the most promising chemicals to target from electrochemical CO_2R. However, there are some critical limitations with the previous models that must be overcome to enable optimized design of CO_2R processes and more accurate prediction of their economic potential.

Firstly, some critical inputs to the existing CO_2R models are too optimistic relative to the best performances demonstrated experimentally for long-term stable electrolyser operation. For example, the study by De Luna et al.[9] used Faradaic efficiencies (FE) for CO of 90 %, current densities (CD) of up to 5000 $A \cdot m^{-2}$, and low overpotentials, which predicted the overall CO_2 energy efficiency more than 60 %. In contrast, there are no public reports of a CO_2 electrolyser simultaneously achieving FE_{CO} above 70% at a current density above 1500 $A \cdot m^{-2}$ for more than 5000 hrs operation (approximately 208 days)[10]. The most stable long-term experiment reported

is from Kutz and co-workers at Dioxide Materials, who maintained a FE_{CO} close to 95% for over six months (4380 hrs) at a current density of only 500 $A \cdot m^{-2}$.[11] Secondly, the existing models tend to oversimply, or even omit, critical relationships between current density, faradaic efficiency, and cell voltage. In a CO_2 electrolyser, the minimum thermodynamic potentials of the CO_2R reactions are independent of current density. However, it's well known that at higher current densities, ohmic losses in the cell components (including the ion exchange membrane) and voltage losses associated with increased overpotentials at the electrode both increase. Therefore, we propose that it's necessary to describe the relationships between current density and cell performance in the model to fully understand how operating conditions affect the product selectivity, energy efficiency, and economics of CO_2R processes.

Thirdly, previous TEA studies[6, 7, 9] used simplified cost factors for the electrolyser that do not permit breakdown costs of individual components such as the cathode and anode catalysts, membrane (including the membrane electrode assembly), bipolar plates, end plates, gaskets, and stack assembly. A more comprehensive and dynamic model for costs of CO_2 electrolysis would provide opportunities to focus scientific efforts to reduce overall costs. For example, replacing noble-metal anode catalysts (e.g., iridium or platinum-based catalysts)[12] with non-noble metal-based[13] or metal-free carbon materials[14] might lead to a more significant impact on overall CO_2 conversion cost than developing new cathode catalysts simply to raise CO selectivities above 90%. Fortunately, the Department of Energy's (DOE's) reports[15, 16] on polymer electrolyte membrane (PEM) electrolysers for H_2 production already provide a comprehensive tool to estimate and analyse the costs of low-temperature PEM-type electrolysers.

We adapted the H_2 electrolysis costing methods for CO_2R electrolysers and added appropriate mathematical relationships to describe CO_2 electrolyser performances at different current densities. Our comprehensive TEA model addresses the three limitations of existing models summarized above and provides material and energy balances that can help identify the critical technical hurdles for developing next-generation catalysts and electrolyser designs. The model is supported by data from bench-scale CO_2R to CO experiments in a vapor-fed two-cell electrolyser stack. In our baseline technology scenario, the projected Levelized cost of CO production was 0.76 $\$ \cdot kg^{-1}$, which is more than 26% higher than the current market price of 0.60 $\$ \cdot kg^{-1}$ CO.[6] Catalyst and membrane costs account for about 35 % of the electrolyzer's capital cost. Unsurprisingly, more than 75% of the operating costs are related to the electricity

required to power the electrolyser. However, when we included the appropriate CD-selectivity-voltage relationships in the electrolyser model, we also observed a somewhat surprising result that the lowest cost CO production was at a current density of only 615 $A \cdot m^{-2}$. In the case that we investigated, operating above 615 $A \cdot m^{-2}$ leads to poorer overall energy efficiency because of the increased hydrogen production (reduced CO selectivity), increased kinetic and concentration losses at the electrodes, and a significant increase in ohmic losses across the membrane.

2 Experimental results used to develop the process model

The CO_2R experiments were performed in a two-cell vapor-fed electrolyser with a cathode prepared from silver nanoparticles on a carbon-based gas diffusion electrode (GDE), an IrO_2-based GDE as the anode, and a Sustainion® anion exchange membrane (AEM) as the separator, as shown in **Figure 1A**. The cathode cell was fed a constant flow of 60 sccm of humidified CO_2, and a flow of 10mM $KHCO_3$ was circulated through the anode chambers. We provide further details on the materials and electrolyser set-up in the Supplementary Information. **Figure 1B** shows the Faradaic efficiencies of CO and H_2 and the cell voltages at current densities from 250 $A \cdot m^2$ to 2000 $A \cdot m^2$. We observed the FE_{CO} decreased from 91.3 ± 1.1 % at 250 $A \cdot m^2$ to 47.3 ± 0.7 % at 2000 $A \cdot m^2$, but the FE_{H2} stayed relatively constant around 2-3%.

Figure 1B also shows that cell voltage (absolute values) increases monotonically from 2.82 V at 250 $A \cdot m^2$ to 3.60 V at 2000 $A \cdot m^2$. The cell voltage values observed here are slightly higher than the values reported for different Ag-based catalysts in a vapor-fed electrolyser.[11, 17] For example, Larrazábal et al.[17] reported a cell voltage of around 3.3 V at 2000 $A \cdot m^2$. The trend in FE_{CO} and cell voltage with the CD is consistent with the findings of Larrazábal et al.[17], who reported a decrease in FE_{CO} and an increase in cell voltages at higher CDs. Although there is a theoretical relationship (Equation S2, Supplementary Information) between cell voltage and CD, we propose a simpler linear equation shown in **Figure 1C** that can adequately correlate the relationship between current density and cell voltage for the purposes of this TEA.

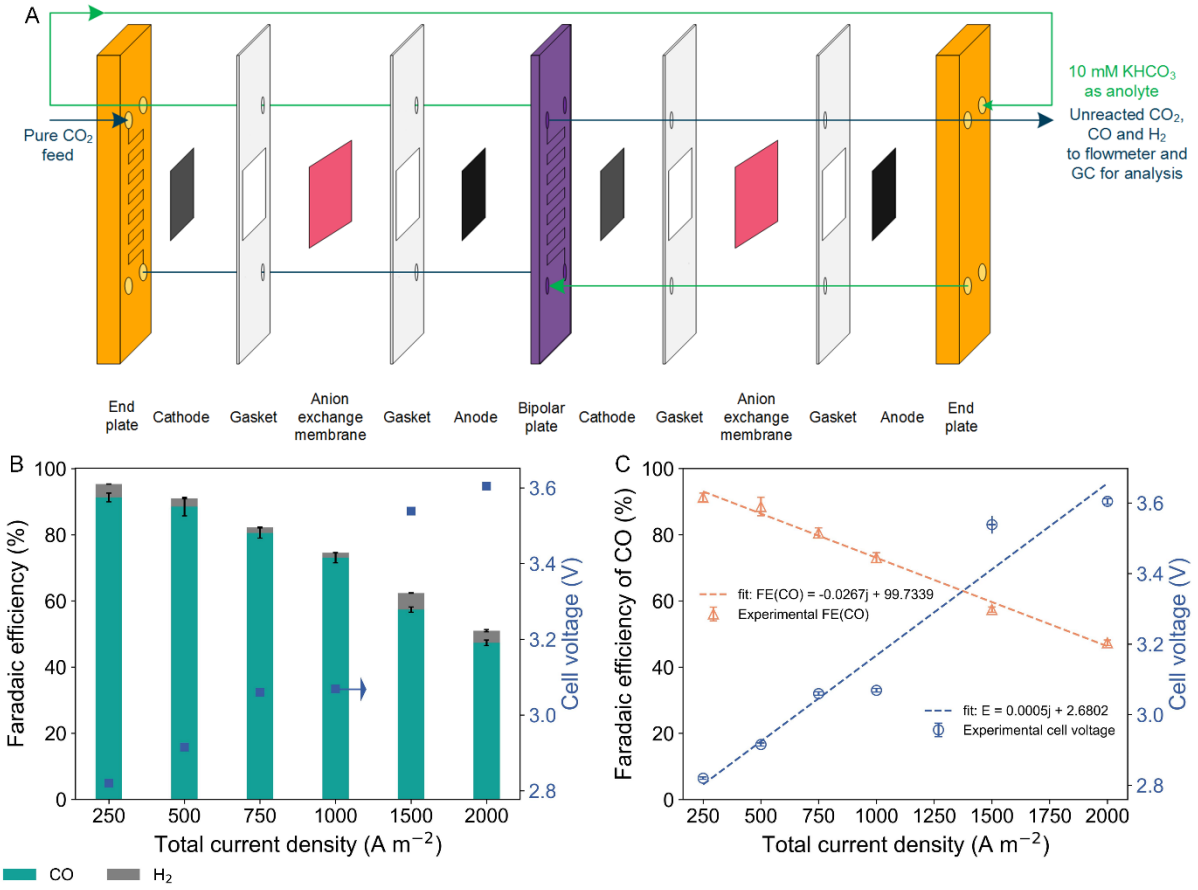

Figure 1. (A) Schematic of vapor-fed CO_2 electrolyser consisting of two cells used in this work; (B) Faradaic efficiency of CO and H_2 and total current density at different cell voltages in a vapor-fed electrolyser. The inlet flow rate of CO_2 was maintained at 60 sccm and anolyte (10 mM $KHCO_3$) was circulated at 1 mL min^{-1}. The error bars show the standard deviation of at least three separate measurements at each current density. (C) linear fitting of faradaic efficiency of both CO and H_2 versus total current density; and cell voltage versus total current density.

Clearly, the CO selectivity in our Ag-GDE electrolyser at 2000 A·m^2 shown in **Figure 1A** is not as high as the results of FE_{CO} close to 90% at 2000 A·m^2 reported by Kutz et al.[11] using a Ag-based GDE cathode or Larrazábal et al.[17] using a porous Ag membrane cathode in a Sustainion®-based vapor-fed electrolyser. We do not claim in this paper to have the best performance for a GDE electrolyser, and we will use the range of results from the literature to help understand the uncertainty in the TEA outcomes. Nonetheless, we provide here some possible explanations of the difference in FE_{CO} at high current density in our study compared to other reports. These include (i) mass transfer and fluid dynamic effects at higher CO_2 flow rates[18] (60 sccm in this study, 100 sccm in Larrazábal et al.[17], and Kutz et al.[11] did not provide flow data), (ii) use of different cathode catalysts and supporting electrodes (20-40 nm Ag NPs deposited on GDL 240 whereas Kutz et al.[11] used Ag NPs (no size mentioned) on a Sigracet

35 BC GDL and Larrazábal et al.[17] used a porous Ag membrane), and (iii) the two-cells in series electrolyser configuration. The use of a two-cell electrolyser in our work could also impact the overall selectivity of CO as the feed going into the second cell contains CO, H_2, and unreacted CO_2 from the first cell, which could reduce the availability of free CO_2 at the cathode surface. A difference in the catalyst particle size may also affect the selectivity and activity of CO_2R.[19-21]

We also highlight that the sum of the FEs of CO and H_2 in **Figure 1B** falls away from 100% at high current density conditions. This mass balance error does not result from an uncontrolled leak from the system nor an unacceptably large experimental error. The first possible explanation for the loss in FE for gas-phase products is the formate production at the cathode (Reaction S8, Supplementary Information), and formate can diffuse through the anion exchange membrane and then be oxidized at the anode (Reaction S14, Supplementary information)[17]. Although we did not detect any formate in the anolyte, Mallouk and co-workers[22] confirmed that formate ions could migrate through the AEM. The rate of formate ions crossover increases at high current densities. The second explanation for FE loss may be a transfer of CO_2 as bicarbonates and carbonates across the AEM (Reactions S10 and S11, Supplementary information), which is a process reported by Seger[17, 23, 24] and Schmidt groups[25]. Seger and co-workers[17] also estimated that the fraction of CO_2 consumption from anion (including bicarbonate/carbonate and formate) crossover through the AEM surpasses the CO_2R to CO, especially at high current densities (> 200 $mA \cdot cm^{-2}$). These two hypotheses are supported by our data in **Figure 2,** showing a fall in the total effluent gas flow rate from the electrolyser at high current densities.

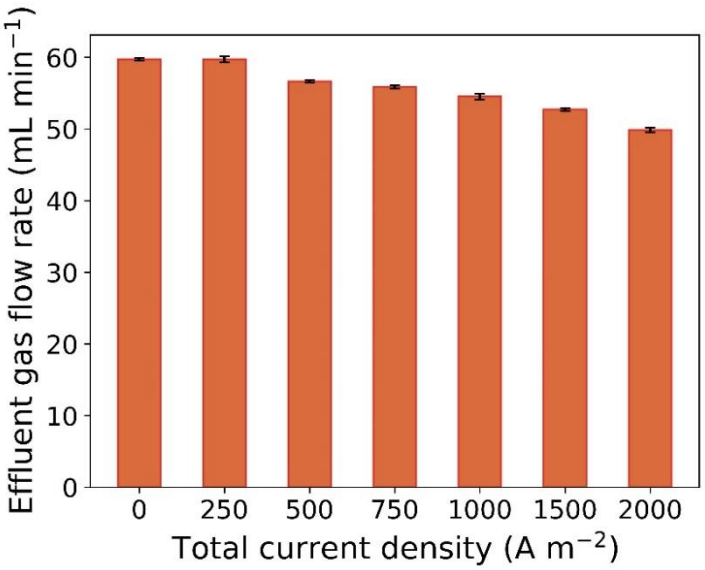

Figure 2. Change in effluent gas flow rate at different current densities in a single-cell set-up. Error bars represent the standard deviation of five different flow-rates.

To evaluate the stability of the Ag-GDE, we performed a CO_2R experiment in a two-cell electrolyser stack at 1000 $A{\cdot}m^{-2}$ for more than 100 h (**Figure 3A**). We observed that the Ag-GDE operates stably for 100 h with FE_{CO} over 60%. After 100 h, the effluent gas flow rate from the cathode cell dropped suddenly. When we took the cell apart after the experiment, we found bicarbonate salts had precipitated in the cathode flow-field (**Figure 3B**), which results from the crossover of potassium ions (K^+) through the AEM due to diffusion and electromigration,[26] after prolonged operation.[18] These solid precipitates fill the pores of the cathode GDE and the flow-field and thus obstructing the effluent gas flow rate and CO_2 flow to the catalyst layer; all of which will eventually leave the electrolyser inoperable.[18, 27] We could restore the electrolyser performance to FE_{CO} above 60% by simply flushing the cathode flow field with deionized water for 10 min. Our 100 h operating times, and even the best results of six months by Kutz et al. [11], are still a long way short of the operating lifetimes for other electrolysers. However, the success of the flushing procedure and the potential for the development of improved AEM materials provides hope that in the future the operating life of CO_2 electrolyser cells can be extended towards the 7 years often achieved by fuel cells and other PEM electrolysers.[28]

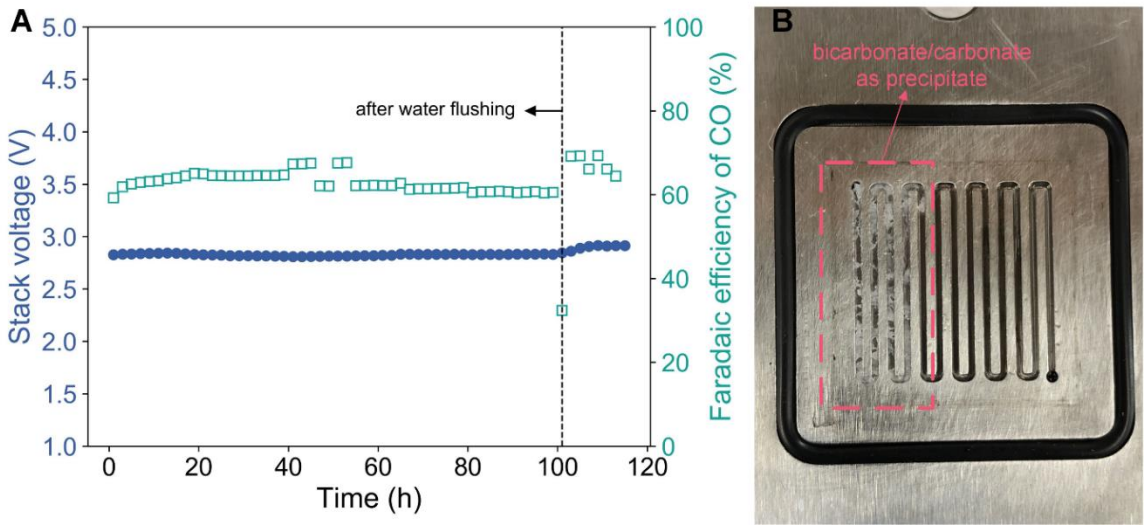

Figure 3. (A) Long-term CO_2R stability test over Ag-GDE at 1000 A·m^{-2} in a two-cell electrolyser. The 10 mM $KHCO_3$ (anolyte) was refreshed every 24 h to keep the maintain the concentrations and conductivity of ions at the anolyte side. The cathode-side was flushed with deionized water after 100 h to remove the precipitation that occurred due to bicarbonate/carbonate in the cathode flow-field as shown in (B).

2.1 Cumulative distribution of voltage consumption in the electrolyser

Figure 4 shows the voltage contributions in the cell due to thermodynamic voltage, kinetic overpotential, mass transport overpotential, and ohmic losses (for more details, see section 1.2 of Supplementary Information). The thermodynamic voltage (E_o) is 1.34 V at all current densities because, in this experiment, the changes in concentrations of the reactant (CO_2) and product (CO) species are too small to have any significant influence on the E_o. The kinetic overpotential increases slightly with current density to be almost 90% of the E_o at 2000 A·m^{-2}. This result highlights the importance of catalyst development to lower overpotentials at high current densities. We estimate that the voltage contribution due to mass transport resistance (aside from ion conduction in the AEM) for this system is negligible at current densities below limiting current density, which is around 2900 A·m^{-2} (calculated from equation S5).

The most significant change in the voltage contributions at high current densities is in the ohmic losses, which rise from 3.99% (0.11 V) at 250 A·m^{-2} to 24.97% (0.90 V) at 2000 A·m^{-2}. These ohmic losses are mostly related to the linear relation between voltage with current density and the resistance to ion transport in the membrane. The polarization results indicate that operating the electrolyser at higher CDs may require a high energy penalty due to high ohmic losses and thus may not be a good option for the economics of the CO_2 conversion to CO. Fornaciari et

al.[29] reported a sharp increase in cell voltages at higher CDs attributed to the dehydration of membranes which causes an increase in ohmic losses in the membranes. Therefore, to reduce the ohmic losses, membrane hydration[29-32] and membranes having extremely low resistances[33] are highly desired.

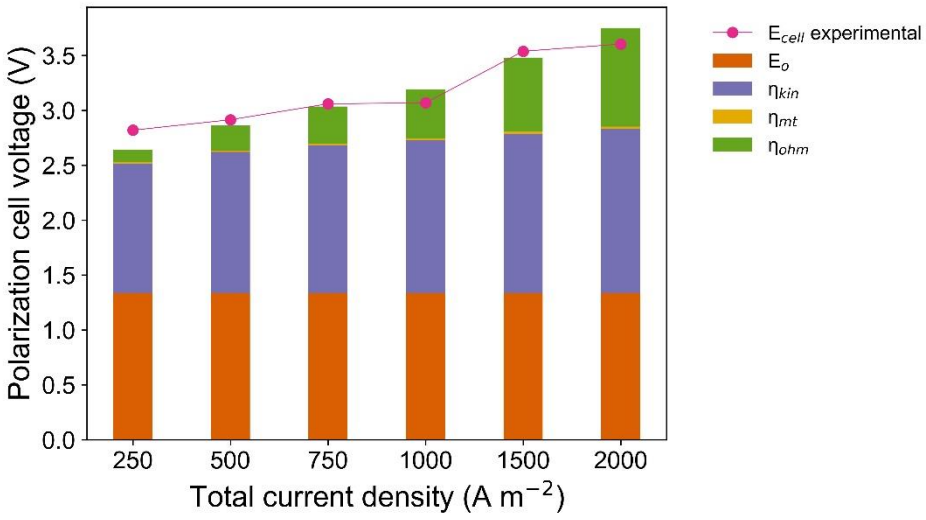

Figure 4. Polarization results showing the cumulative voltage (absolute value) breakdown including the thermodynamic voltage, kinetic overpotential, mass transport overpotential, and ohmic losses. Where kinetic overpotential was calculated from Equation S4 and exchange current density (j_o) was assumed as 0.1 A·m^{-2}.

3 Results from the TEA model

Based on the mass-balance equations presented in the Supplementary Information, a block flow diagram showing molar flow rates of inlet and outlet streams of the CO_2 electrolyser and separator unit for CO_2R to CO under the baseline parameters is shown in **Figure 5**. The single-pass conversion of 50% was pass conversion (50%) was based on recent progress made by Jeng and Jiao[34] to achieve 43% CO_2 single-pass conversion in a flow electrolyser. **Table 1** presents the list and values of key operational, design, and input parameters assumed for the TEA model in the baseline scenario. The price of captured CO_2 to feed the electrolyser of 60 \$·ton^{-1} CO_2 was based on the lower end of the range of capture costs for the power sector from a US Department of Energy report.[35] The stack replacement time of 7 years[36] was based on the current stable performance of PEM electrolysers. The concentrations of gas effluent from CO_2 electrolyser are 42.21 vol% CO_2, 42.21 mol% CO, and 15.58 mol% H_2. Based on these concentrations, the gas separation required in this process could be a similar process to that used in the upgrading of biogas.[37] Bauer and co-workers[38] identified pressure swing

adsorption (PSA) as a potential technique to remove more than 99% CO_2 from the biogas feed stream. The discussion on choosing the right separation technique for $CO_2/H_2/CO$ separation is outside the scope of this work. We used the shortcut PSA approach to provide a rough estimation of the gas separation cost for simplicity. For a more detailed economic analysis of gas separation using PSA, we refer the readers to articles by Ho et al.[39, 40], Zhao et al.[41], and Kim et al.[42].

Table 1. Input parameters (including operating, design, cell, and economic parameters) for the TEA model assumed in the baseline scenario.

Parameters	Value	Reference
Current density ($A \cdot m^{-2}$)	1000	This work
Single-pass CO_2 conversion (%)	50	[18, 34]
Electrode lifetime (days)	340	Assumed
Cathode loading ($kg \cdot m^{-2}$)	0.02	This work
Anode loading ($kg \cdot m^{-2}$)	0.01	This work
Stack replacement (years)	7	[36]
Stack replacement cost (% of the installed capital cost)	15	[36]
Price of cathode ($\$ \cdot kg^{-1}$)	800	Alibaba website
Price of anode ($\$ \cdot kg^{-1}$)	120,000	Hongwu International Group Ltd. China
Price of the membrane ($\$ \cdot m^{-2}$)	325	See section 2.3.2 in Supplementary
Price of CO ($\$ \cdot kg^{-1}$)	0.60	[43]
Price of electricity ($\$ \cdot kWh^{-1}$)	0.06	[44]
Price of captured CO_2 ($\$ \cdot ton^{-1}$ CO_2)	60	[35]
Price of water ($\$ \cdot m^{-3}$)	1.43	[6]

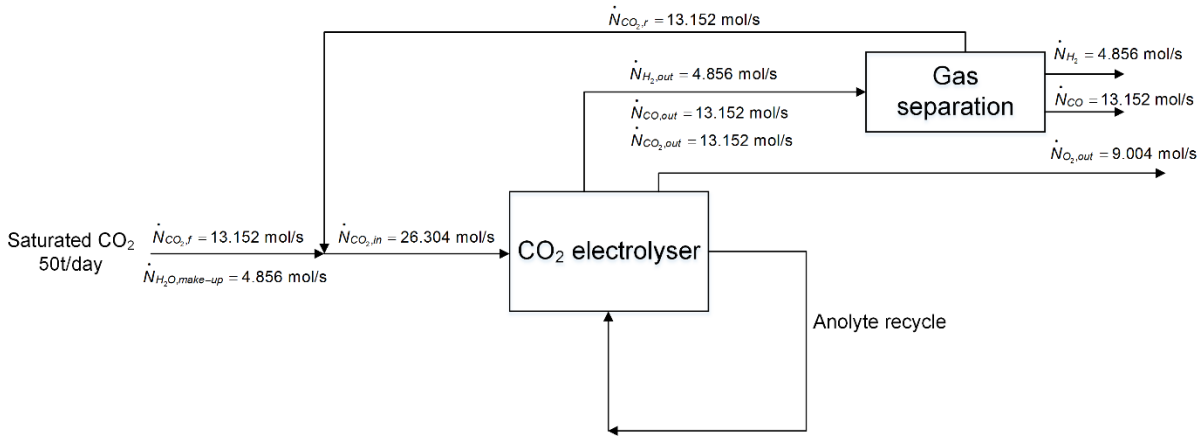

Figure 5. Molar flow-diagram for CO_2R to CO under the baseline parameters.

3.1 **Levelized cost of CO production in the base case**

Table 2 summarises the capital equipment costs and key operating costs for an electrolyser and gas product separation process to convert 50 tons per day of CO_2 to CO using the base case input data from Table 1. A comparative analysis of our electrolyser's capital cost with other literature reports is also presented in section 2.3.1 of the Supplementary Information. The direct costs of the electrolyser including the MEA, catalysts, stack assembly, stack testing and conditioning equipment, gaskets, bipolar plates, and end plates contribute around one-third of the total equipment costs for the process ($10.15 million). The product gas separation by PSA accounts for approximately 17.09 % of the installed equipment cost.

The MEA, which in this analysis includes the gas diffusion layers and the anion exchange membranes, is the largest single component cost in the electrolyser stack (18.45%) and most of this cost is the membrane material. In our lab experiments, we used Sustainion® X37-50 from Dioxide Materials (USA) as the AEM. At present, Sustainion® AEM patented by Dioxide Materials is considered to provide better performance than other membranes attributed to its low area-specific resistance and high stability for longer durations under alkaline conditions.[45] The price per m^2 of Sustainion® X37-50 that researchers currently pay (~ 3432 $\$\cdot m^{-2}$ from dioxidematerials.com) for lab-scale quantities is not a good prediction of the future cost for large-scale CO_2 electrolyzers. Therefore, we used a learning curve analysis (Section 2.3.2 of the Supplementary Information) based on the historical prices of Nafion[46] to estimate a more representative future price for an AEM of 325 $\$\cdot m^{-2}$. This price is around five times the current price of the Nafion cation exchange membrane.

The catalyst cost is almost entirely dependent on the cost of the IrO_2 at the anode (120,000 $\$\cdot kg^{-1}$ from Hongwu International Group Ltd. China)[47], which accounts for $4.17 million. The Ag nanoparticles (800 $\$\cdot kg^{-1}$ from the Alibaba website[48]) at the cathode add only 1.32% to the catalyst cost. This result is consistent with Masel et al.'s recent report that cathode catalysts contribute less than 4% of the cost of the membrane electrode assembly[10]. The cost analysis here highlights that developing (1) low-cost alternatives to IrO_2-based anode catalysts and (2) low-cost, high-performance AEMs are critical challenges for CO_2 electrolysis. Unsurprisingly, the cost of electricity to drive the electrochemical reactions was the most significant operating expense in the base case scenario (77.36% of OPEX).

Table 2. Estimated capital equipment costs and operating costs for the electrolyser and pressure swing adsorption system for product separation to convert 50 t/day of CO_2 to CO in the base case scenario described in Table 1.

Capital equipment costs	$ million	% of CAPEX
Membrane assembly (GDL + AEM)	4.80	18.45
Pressure swing adsorption (PSA) units	4.45	17.09
Catalyst (cathode and anode)	4.23	16.23
Stack assembly	0.37	1.43
Stack testing & conditioning	0.36	1.40
Bipolar plates	0.26	1.00
Gaskets	0.10	0.37
End plates	0.02	0.10
Balance of Plant	11.44	43.94
Total CAPEX	26.04	

Operating costs	$ million/year	% of OPEX
Electrical energy	5.39	77.36
CO_2 feed cost	1.02	14.64
Pressure swing adsorption (PSA) units	0.34	4.81
Stack replacement	0.22	3.14
Water consumption	0.004	0.05
Total OPEX	6.97	

Using these CAPEX and operating cost estimates with the scenario described in **Table 1** over a 20 year plant lifetime, we estimated the Levelized cost of CO production to be around 0.76 $\$\cdot kg^{-1}$, which is 26.7% higher than the current market price of 0.60 $\$\cdot kg^{-1}$ CO. **Figure 6** highlights that nearly 63% or 0.48 $\$\cdot kg^{-1}$ CO is due to the cost of the electricity (at 0.06 $\$ kWh^{-1}$) required to power the electrolyser. The cost of electricity is almost ten times the stack capital and six times the cost of the balance of the plant. The next most significant contributor to the cost of CO production is the cost of CO_2 feed capture (12%). Costs of stack replacement, PSA (both capital and operating), and water consumption are each contributing less than 10% of the total CO production cost. The tornado plot in **Figure 7** highlights that the cost of CO production is most sensitive to the electricity price. Even a one-cent decrease in the electricity price from the base value to 0.05 $\$ kWh^{-1}$ reduces the CO production cost by around 11.5% (i.e. 0.68 $\$\cdot kg^{-1}$).

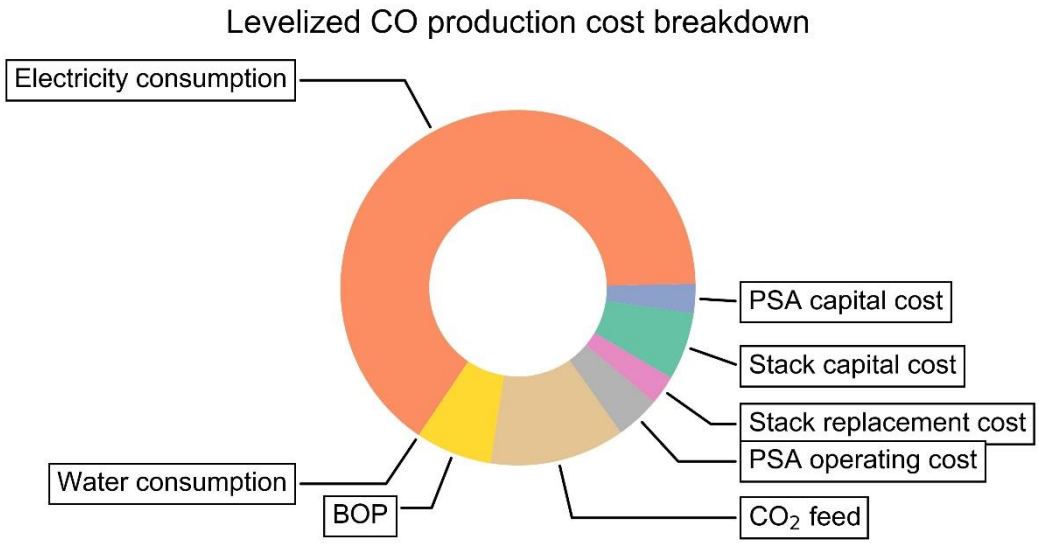

Figure 6. Levelized CO production cost breakdown under the baseline scenario. The estimated Levelized CO production cost is 0.76 $\$\cdot kg^{-1}$ as compared to 0.60 $\$\cdot kg^{-1}$ market price of CO.

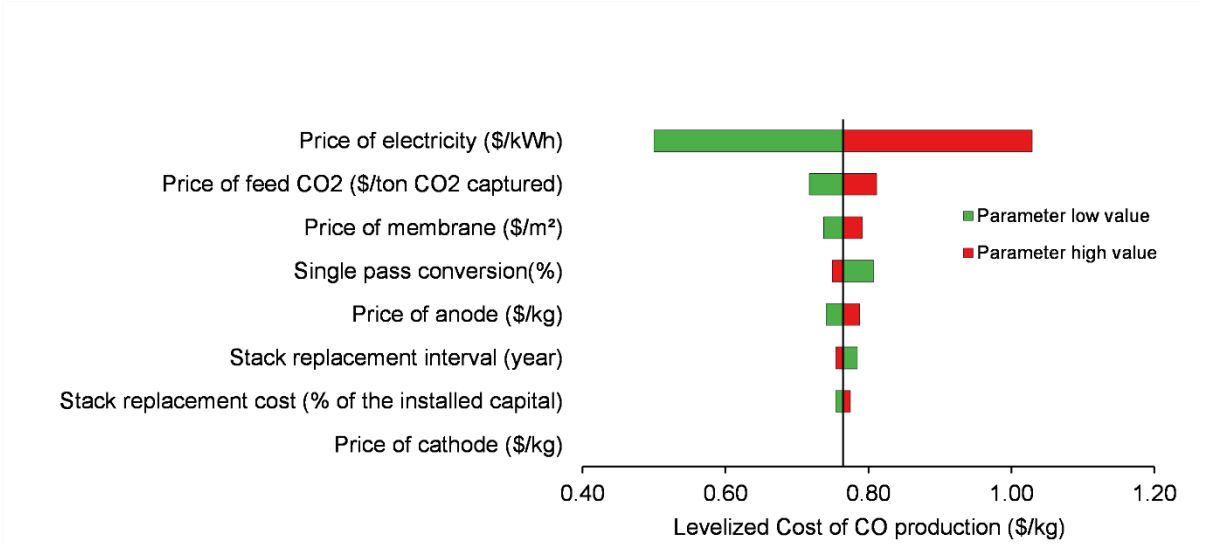

Figure 7. Sensitivity analysis of the Levelized cost of CO production from CO_2R. The data on the range of parameters are mentioned in Table S3.

3.2 How does maximizing current density affect the economics of CO_2 to CO electrolysis?

Masel et al.[10] and Burdyny and Smith[49] have suggested that to achieve commercial viability pilot-scale CO_2 electrolysers for CO production need to operate stably at a current density greater than 2000 $A \cdot m^{-2}$ for periods of 3-7 years, similar to other PEM electrolysers. However, few CO_2R electrolysers have achieved this current density benchmark for periods of 100 – 200 hrs, and very few electrolysers[11] have operated stably for more than six months (4380 hrs) even at current densities below 2000 $A \cdot m^{-2}$. We wanted to better understand the impacts of the current density, and the significance of the targets like 1000 - 2000 $A \cdot m^{-2}$, on the Levelized cost of CO production when the costs of product separation are also included in the analysis. In this test, we varied the only current density from 250 to 2000 $A \cdot m^{-2}$ and used the electrolyser performance relationships described in Section 2 to estimate the cost of CO production as shown in **Figure 8A**. In Region 1 (green) of **Figure 8A** from 250 $A \cdot m^{-2}$ to 615 $A \cdot m^{-2}$ the Levelized cost of CO production decreased from 0.85 to 0.72 $\$ \cdot kg^{-1}$. At these current densities, the selectivity for CO is high (FE_{CO} > 90%), but the reaction rate is slow (see **Figure 1B**), so a large electrode area is required to convert the specified 50 t/day of CO_2 to CO. This relationship between current density, reaction rate, and electrolyser area (which directly impacts costs of the MEA, catalysts, and BOP) explains why the CO production cost falls in Region 1.

However, at current densities above 615 $A \cdot m^{-2}$, Region 2 (red) shows the Levelized cost of CO production begins to increase at higher current densities. **Figure 8B** illustrates the increase in CO production costs above 615 $A \cdot m^{-2}$ arises from increased ohmic losses, increased energy losses and electrode areas associated with H_2 evolution, and greater overpotentials including kinetic and mass transfer overpotentials required to maintain the high current density. These factors all contribute to increasing the electricity consumption in the electrolyser. The increased ohmic losses at high current density are mostly associated with resistance to ion transport in the AEM, as described by Salvatore and Berlinguette[50]. In this scenario at currents above

615 A·m^{-2} the additional power consumption costs begin to outweigh any cost savings from reduced electrode areas at higher current density.

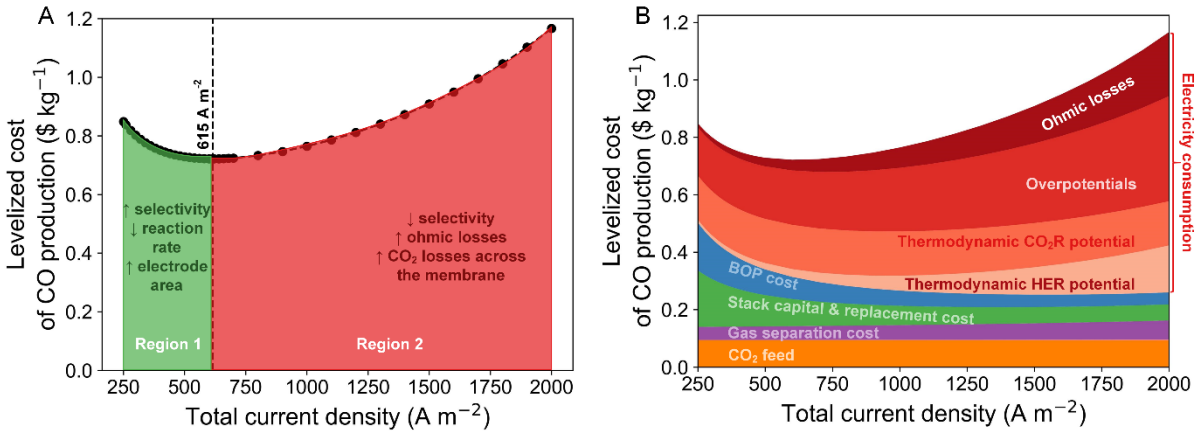

Figure 8. (A) Variation in the Levelized CO production cost as a function of current densities and (B) breakdown of the Levelized CO production cost in terms of different cost parameters as a function of current densities. Here in (A) and (B), both the cell voltage and faradaic efficiency of CO were linearly correlated as a function of current density as shown in Figure 1(C). Symbols ↑ and ↓ represent high and low values of parameters in (A).

An additional effect on electrolyser sizing of the HER increase at higher current densities is that the fall in CO selectivity (see **Figure 1C**) leads to an increase in the electrode area required to convert the 50 t/day of CO_2 in this scenario. This result demonstrates a clear trade-off between the benefits of increasing the current density and the disadvantage of losing the CO selectivity on the required electrode area. Based on our experimental data at 2000 A·m^{-2}, the CO selectivity falls below the target threshold of FE_{CO} = 50%. In Section 3.3.1, we explore how maintaining CO selectivity above 90%, for example, by improved cathode catalysts might allow the minimum Levelized cost of CO production to be shifted to a higher current density.

Another disadvantage of losing the CO selectivity at high current densities is the increasing product separation cost because of having diluted product in the feed stream to the gas separator (PSA) which makes the process costlier to achieve a similar product separation efficiency. **Figure 8B** shows a slight increase in the gas separation cost (both operating and capital) with the current density because our PSA model only accounts for cost related to the input flow rate (m^3/h) of the feed[37] and does not take into account the mole fraction of the product in the feed (for more details, see Supplementary Information section 2.3.3). To address this issue, we used the Sherwood plot to estimate the gas separation cost by involving the concentration of product as a function of cost. It is important to note that the cost estimation from the Sherwood plot

only provides a single separation cost which includes profit margin, capital, and operating cost; and it does not include how much input flow rate of feed is treated (or processed). From the Sherwood analysis, we found that gas separation cost also increases slightly with the increase in current density. Surprisingly, both the capital and operating costs of PSA were almost two orders higher than the total gas separation cost calculated from the Sherwood plot. The low gas separation cost in the Sherwood plot may be attributed to the low gas separation factor (0.001 $\$\cdot kg^{-1}$) taken in our work. Therefore, given the uncertainties around the costing methods of the gas separation, we expect the actual gas separation cost to be even higher. For specific project evaluations, a more detailed gas separation model may help identify the optimum process parameters (current density or voltage) at which the CO_2 electrolysers should be run to minimize the energy losses associated with the separation processes.

In addition, the operation at high current density increases CO_2 losses due to the high local pH at the cathode[49, 51] and thus allowing hydroxide ions to react with CO_2 to form bicarbonates/carbonates which crossover to the anode through the AEM (see section 2.1 for more details).[17] The co-evolution of CO_2 with O_2 at the anode indicates the need for additional separation units to recover the CO_2 and recycle it back to the cathode, making the overall process more expensive.[17, 23] The long-term stability of the CO_2 electrolysis owing to the formation of solid precipitation at the cathode (see discussion on **Figure 3B**),[52] degradations of AEM,[11] and change in electrode structures is another concern where none of the reported AEM-based CO_2 electrolyser studies have shown stable CO_2R performance for more than 6 months.[11] For instance, AEMs, at high current densities, are prone to dehydration which could cause high ohmic losses and performance degradation, affecting ion and water transport.[32] Bicarbonates and carbonates migrating through the AEMs have lower (3-4x)[53] dilute solution mobilities than the hydroxide, resulting in low conductivity of the AEM. Moreover, the lifetimes of the AEMs are limited by the innate instability of the membrane materials in highly alkaline media – with hydroxyl ion, being a strong nucleophile,[54] attacks both the anchored cations and polymeric backbone of the AEM, leading to multiple degradation pathways.[55] Whereas, at the anode, high current density allows water oxidation to produce more protons which makes the anolyte more acidic, resulting in anodic corrosion (or dissolution of the anode catalyst).[33]

3.3 **Opportunities to reduce the CO production cost**

Based on the sensitivity analysis above, **Figure 9** demonstrates potential pathways/opportunities to reduce the Levelized cost of CO production to below 0.60 $\$\cdot kg^{-1}$. A low price of electricity is an important characteristic of any potential pathway to 0.60 $\$\cdot kg^{-1}$ CO, and Scenario 2 shows the outcome if the forecast renewable electricity price of around 0.03 $\$\cdot kWh^{-1}$ is achieved through continuous development of low-cost and large-scale renewable technologies.[85] Scenario 3 shows an optimistic forecast if the CO_2 electrolyser performance can be pushed to achieve 90 % CO selectivity at 2000 $A\cdot m^{-2}$ and 3 V for at least 10 years stack lifetime, and the costs of catalysts and membranes can be reduced. This scenario indicates the potential benefits of targeted research and development strategies for CO_2 electrolysis. As engineers/electrochemists, the enhancement in electrolyser performance parameters is something we can control by focusing on the development of (a) more selective and efficient cathode catalysts; (b) efficient reactor design for low voltage losses; (c) novel capture solvents to reduce the cost of captured CO_2 from industrial sources; (d) low-cost anode catalysts; and (e) cheap and stable anion-exchange membranes. Whereas, changes in the economic parameters are regulated by policymakers and the market. The impact of electricity prices on CO cost is as significant as the opportunities available to improve the technical parameters of the electrolyser. Scenario 4 in **Figure 9** shows that if both the electrolyser performance improvements can be achieved and the cost of electricity falls to 0.03 $\$\cdot kWh^{-1}$, then the Levelized cost of CO production could potentially fall to as little as 0.30 $\$\cdot kg^{-1}$. In the following section, we will talk about different opportunities to reduce the cost of CO production from both the electrolyser's performance and economic parameters perspective.

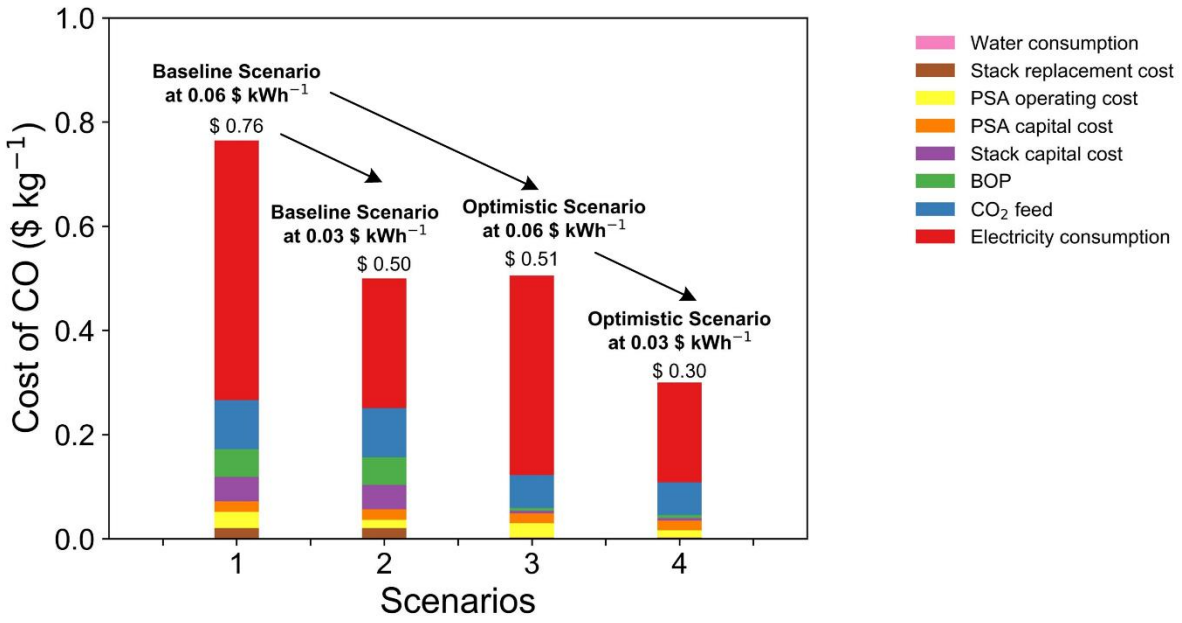

Figure 9. Waterfall chart highlighting pathways towards reduced CO cost through CO_2R. The optimistic scenario assumed a current density of 2000 A·m^{-2}, FE_{CO} of 90%, cell voltage of 3 V, stack replacement interval of 10 years, stack replacement cost (10% of the installed capital cost), 600 $·kg^{-1} cathode and anode catalyst price, 40 $·ton^{-1} CO_2 feed cost, and 100 $·m^{-2} cost of the membrane. The rest of the parameters are unchanged and their values are the same as those mentioned in Table 1 (base values).

3.3.1 Maintaining high CO selectivity at high current densities

Product selectivity, by definition, is the ratio of the theoretical amount of charge needed to form a product (CO in our case) over the total charge supplied by the electrical current in making the same amount of product. Therefore, one way to keep the energy consumption as low as possible is to maintain high CO selectivity, especially at high current operations. Although we could only achieve 47.3% CO selectivity in our electrolyser at 2000 A·m^{-2}, there are reports demonstrating over 90% CO selectivities at current densities above 2000 A·m^{-2}. For example, Larrazábal et al.[17] operated their CO_2 electrolyser at 2000 A·m^{-2} for CO selectivity over 90% using commercial Ag membranes. Similarly, Lee et al.[56] reported a CO selectivity close to 90% at 3120 A·m^{-2} in a vapor-fed electrolyser employing coral-nanostructured Ag GDEs. Further increasing the current densities to 5000 A·m^{-2} could lead to dehydration of membrane and large ohmic losses in the electrolyser.[10]

Nonetheless, continued advances in catalysts are leading to reports of high selectivity at higher currents without significant increases in cell voltages.[57, 58] Therefore, we considered how these developments in cathode catalysts and reactor design could potentially lower the cost of CO

production by improving the CO selectivity especially at high current density Here we assume that the cathode catalyst could maintain a stable CO selectivity at 90% under the same experimental conditions (i.e. between 250 and 2000 $A \cdot m^{-2}$). **Figure 10** shows that maintaining CO selectivity at 90% allows the electrolyser to operate at an optimum current density of 1350 $A \cdot m^{-2}$ at which the Levelized cost of CO production was reduced to 0.565 $\$ \cdot kg^{-1}$ (lower than the current market price of CO). Further increasing the current density (beyond 1350 $A \cdot m^{-2}$) increases the CO production cost because ohmic losses in the AEM start to dominate, meaning that the electricity consumption due to ohmic losses costs more than the decrement in cost from the reduction in electrode area. The results of CO production cost at high CO selectivity again highlight our hypothesis that it is not always economical to operate the electrolyser at high current densities and is important to understand how ohmic losses in the electrolyser (especially the AEM) increase at high current operation.

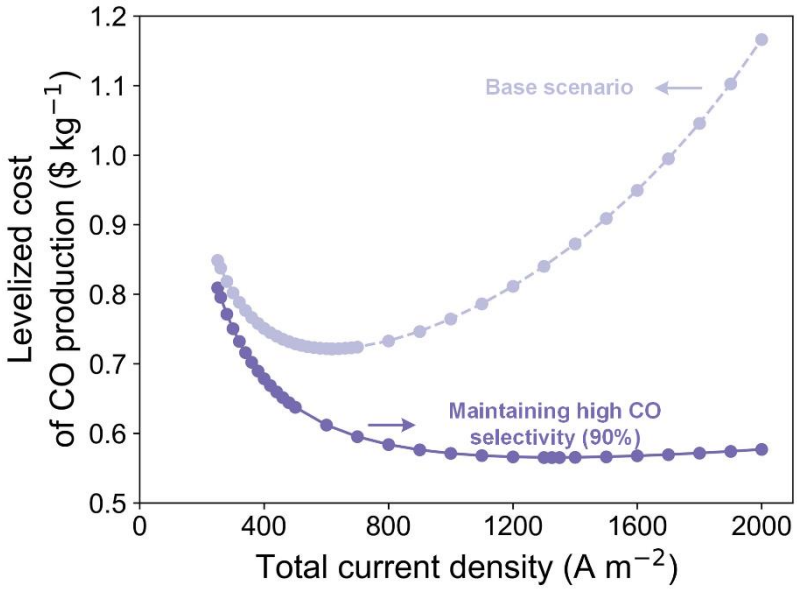

Figure 10. Variation in the Levelized cost of CO production with current density (assuming the CO selectivity remains stable at 90% at all current densities, while cell voltage follows the same correlation with the current density as reported in Figure 1C).

3.3.2 Lowering the energy consumption of the electrolyser

The energy consumption of an electrolyser is directly proportional to the cell voltage. And as mentioned in section 2.1, the voltage required to run the electrolyser at a required current density is a summation of thermodynamic equilibrium potentials of the cathode and anode reactions, their kinetic overpotentials, concentration overpotential of reactants, and ohmic

losses associated with the AEM. Reducing the thermodynamic equilibrium potentials and improving the electrolyser losses (overpotentials) could decrease the cost of CO production.

The thermodynamic equilibrium potential is the minimum thermodynamic voltage to drive the electrolysis reactions at the cathode and the anode. In our model, the equilibrium cell potential for CO_2R to CO at the cathode and OER at the anode is 1.34 V, whereas, the equilibrium cell potential for HER at the cathode and OER at the anode is 1.23 V. In both CO_2R to CO and HER, a large part of the energy consumption is related to the OER at the anode, contributing 1.23 V to the equilibrium potential. Therefore, coupling CO_2R with reactions having low potentials than OER could facilitate the reduction of overall energy consumption in the electrolyser. Many organic reactions, especially alcohol oxidation, occur at lower potentials than OER in aqueous electrolytes and do produce a valuable product without the expense of extra energy. For more information on value-added anodic reactions, we refer the readers to recent articles by Na et al.[59] and Endrődi and Janáky[60]. For example, ethanol oxidation to acetaldehyde happens at a half-cell potential of 0.193 V,[61] meaning an almost 84% saving in energy consumption at the anode. Additionally, acetaldehyde sells at a market price of 1 $\$\cdot kg^{-1}$,[62] a much higher market price than oxygen (0.024 – 0.04 $\$\cdot kg^{-1}$)[63] and even higher than the market price of CO (0.60 $\$\cdot kg^{-1}$)[6]. However, ethanol itself is expensive (market prices vary between 0.4 – 0.75. $\$\cdot kg^{-1}$)[59, 60] Therefore, we need to look at chemicals that are either cheap or available freely as a waste product from an industrial stream and simultaneously have lower oxidation potentials.

One such chemical is glycerol, which is available cheaply as a byproduct of biodiesel production.[44] The equilibrium half-cell potential of glycerol oxidation to glyceraldehyde is 0.41 V, while glycerol to lactic acid is 0.25 V.[44] So, coupling glycerol oxidation with CO_2R to CO in an electrolyser could save electrical energy between 66 and 80% (depending on the type of product produced from glycerol). **Figure 11** shows how the Levelized cost of CO production reduces at different current densities when CO_2R is coupled with glycerol oxidation to lactic acid at the anode. Even though there exist distinctive challenges with different anodic reactions including slow reaction kinetics, side reactions, and downstream separation, coupling CO_2 electrolysis with other anode reactions[44, 60, 64] have great potential to reduce the overall energy consumption and thus should be further investigated.

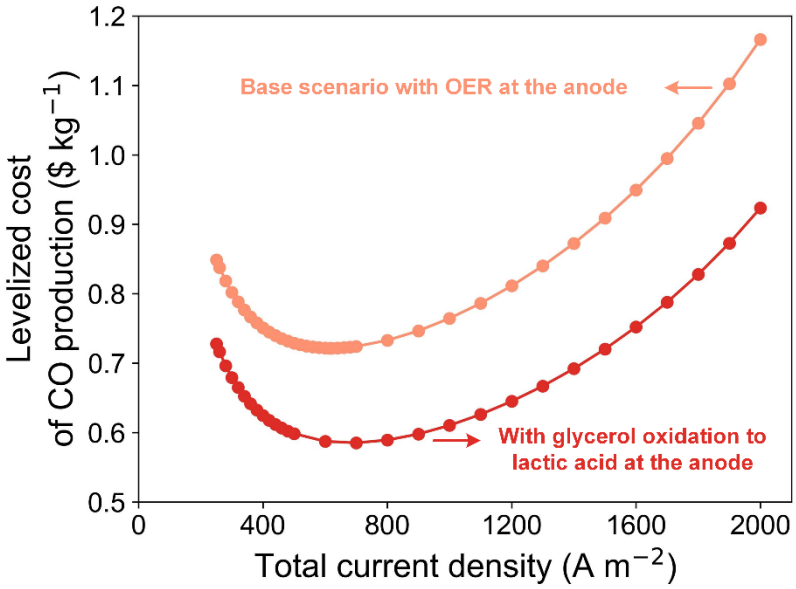

Figure 11. Variation in the Levelized cost of CO production with the current density when OER at the anode was changed to glycerol oxidation to lactic acid.[44] The equilibrium half-cell potential of glycerol to lactic acid is 0.25 V.

In addition to reducing thermodynamic equilibrium potentials, lowering electrolyser losses associated with the overpotentials could improve the energy efficiency of the CO_2 electrolysis. With the increase in the current density, overpotential related to the mass transfer limitations of the reactant delivery to the electrode surface does not change much, while, kinetic overpotential arising from sluggish reaction kinetics at the electrode surface increases slowly (see **Figure 4** and **Figure 8B**). From our CO_2R experiments, we found an onset cell potential of 2.68 V (see cell voltage-current density relationship equation in **Figure 1C**), meaning the contributions of kinetic losses from both the anode and the cathode are nearly 1.34 V, the same as thermodynamic equilibrium potential. In the last decade, researchers have made substantial progress to enhance both CO_2R and OER catalysts with low overpotentials and high selectivities by altering the design principles of the catalyst, as reviewed elsewhere by Gao and co-workers[65] for CO_2R to CO cathode catalysts and by Xu and co-workers[66] for OER catalysts. **Figure 12** shows decreasing the kinetic loss at the cathode and the anode by half brings the Levelized cost of the CO curve down by almost 0.14 $\$\cdot kg^{-1}$, however, we did not observe any change in the trend of the Levelized cost of CO with current density.

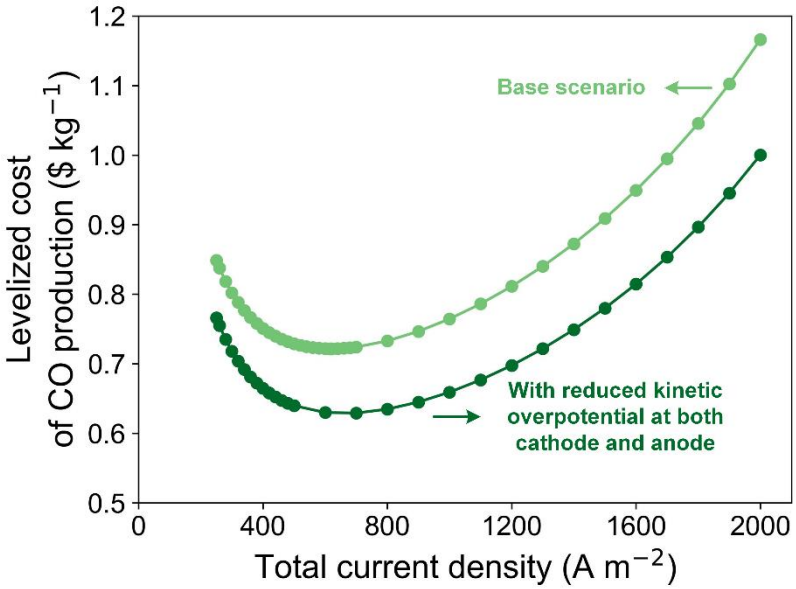

Figure 12. Variation in the Levelized cost of CO production with current density when the overall kinetic overpotential is reduced by half (including reactions happening at both cathode and anode). The rest of the parameters remained unchanged to that in the baseline scenario.

The final opportunity to reduce energy consumption could be to minimize ohmic losses due to the low ionic conductivity of the AEM. The hydroxides, bicarbonates, and carbonates are the main charge carriers transported across the AEM during CO_2R,[17] suggesting that an AEM having high conductivity for these ions could improve the ohmic losses. In 2017, Masel and co-workers[11] developed state-of-the-art Sustainion® AEMs that have higher conductivities and stabilities in alkaline conditions than other commercial membranes including Fumasep (from Fumatech), A201 (from Tokuyama), and Orion TM1 (from Orion Polymer).[67] For instance, the Sustainion® AEM has an ionic conductivity of 80 mS·cm^{-1} (Sustainion 37-50 in 1 M KOH at 30˚C)[68] as compared to 40 mS·cm^{-1} (OH) in Fumasep (FAA-3-30)[67], 42 mS·cm^{-1} (OH) in A201[67], and 54 mS·cm^{-1} (OH) in Orion (Pure material m-TPN1)[69]. At present, many researchers used Sustainion® AEMs in their work to achieve high product selectivity at high current densities and low cell voltages using different catalysts.[18, 70-74]

Figure 13 demonstrates how an increase in ionic conductivity of the AEM decreases the Levelized cost of CO production, especially at higher current densities because ohmic losses follow a linear progression with the current density. Moreover, ohmic losses could be reduced by decreasing the membrane thickness which decreases the membrane resistance itself. However, it might be possible that decreasing the membrane thickness could affect its chemical and mechanical stability,[75] and thus difficult to handle during CO_2R operation. Given the

catholyte-free and zero-gap configuration of the CO_2 electrolyser, we also need to develop strategies to improve the catalyst-membrane interfaces for better ion conduction (or low ohmic losses).[33]

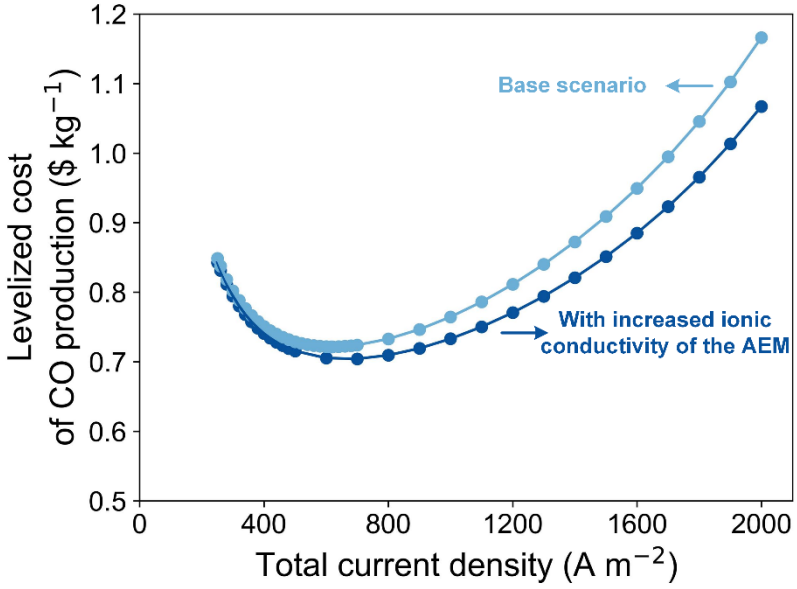

Figure 13. Variation in the Levelized cost of CO production with current density when the ionic conductivity of the AEM is increased by almost double. The rest of the parameters remained unchanged to that in the baseline scenario.

Using low-value waste heat sources in an industrial complex to heat the electrolyser to temperatures of 40 - 80˚C could be another way to reduce electricity requirements. Performing the CO_2 electrolysis at a slightly higher temperature could lower the thermodynamic potentials and kinetic overpotentials at the cathode and the anode, and a drop increases the conductivities of the electrolyte and membrane[76]. For example, Dufek et al.[77] reported approximately a 35% reduction in the overall cell voltage for CO_2R when the cell temperature was increased from 18˚C to 70˚C. However, there may be other performance trade-offs to operating at higher temperatures because the product selectivity may be reduced due to CO_2 mass transport limitations and promoted competitive HER.[76] Therefore, it is important to consider how the effect of temperature on product selectivity and energy consumption affects the overall economics of CO_2R to CO.

Another way to reduce voltage losses is by performing high-pressure CO_2 electrolysis. According to the Nernst equation, high pressure increases the thermodynamic equilibrium voltage.[78] In industrial electrolysers, the use of high-pressure may be justified if the cost savings from achieving the highest possible current density and enhanced electrolyser

efficiency outweigh the extra costs of compression and construction of higher pressure equipment.[79]

3.3.3 Reducing CO_2 feedstock cost or implementing carbon taxes

Our results show clearly how the price of CO_2 feed impacts the Levelized cost of CO production. Raksajati et al.[80] reported that the cost of post-combustion CO_2 capture from flue gases can be reduced to 40 $\$\cdot ton^{-1}$ CO_2 captured with developments in novel solvent/absorber formulations, process design, and intensification. Our results in **Table 1** show this CO_2 capture cost reduction leads to a 4% drop in the Levelized cost of CO production compared to the baseline scenario. To encourage a shift towards low CO_2 emissions technologies, a carbon credit or tax must be allocated to CO_2. The current carbon prices are around 10 $ per ton of CO_2 equivalent (tCO_2e^{-1}) whereas the future carbon prices could rise to 100 $\$\cdot tCO_2e^{-1}$ to restrict warming below +2˚C.[81] In case a carbon price of 100 $\$\cdot tCO_2e^{-1}$ would be taken into account, the CO cost could be further reduced to 0.61 $\$\cdot kg^{-1}$, very close to the market price of CO (0.60 $\$\cdot kg^{-1}$).

3.3.4 Developing lower cost anode catalysts and anion exchange membranes

The anode catalyst and the membrane are the most expensive components in the electrolyser (Table 2). **Figure 7** shows that a 50% reduction in the price of the anode catalyst can have a significant effect on the CO production cost. The influence of anode catalyst price suggests that it would be beneficial for a commercial electrolyser to have an anode catalyst based on abundant metals which could show similar catalytic performance to that of a precious anode catalyst (IrO_2-based). Potential alternatives to IrO_2-based anode catalyst could nickel-based[82, 83] anodes.

The high price of the Sustainion® membrane also affects the CO production cost. For example, if the current price (325 $) of the membrane can be reduced to 100 $ (similar to the price of a new perfluorinated membrane recently patented by Kazacos and Kazacos[84] from the University of New South Wales, Australia), we could obtain a CO production cost of 0.73 $\$\cdot kg^{-1}$. Currently, the Sustaionion® AEMs used in CO_2R experiments are produced at a small scale but with increased demand and production volume, the cost of this membrane is expected to drop even lower.

4 Conclusions

Here we present an experimental and TEA model to assess the feasibility of CO production from CO_2R. Experimental CO_2R results show that at higher current densities Ag gas diffusion electrodes may produce large amounts of formic acid which diffuses towards the anode side through the anion exchange membrane (AEM). We observed a loss in the effluent flow rate of gas from the cathode side attributed to the transfer of CO_2 through the AEM to the anode side in the form of carbonates/bicarbonates especially at high current densities > 1000 $A \cdot m^{-2}$. However, we did not consider the formation of formic acid and loss of CO_2 in the mass balance of the TEA model. Based on the current electrolyser performance and characteristics, we estimated a Levelized CO production cost of 0.76 $\$ \cdot kg^{-1}$ over 26% higher than the present market price of 0.60 $\$ \cdot kg^{-1}$ CO.

Further investigation into the TEA model provides several conclusions. For instance, operating electrolyser at high current densities ($\geq$ 1000 $A \cdot m^{-2}$) may increase the CO production cost due to a linear increase in ohmic losses at the AEM, marginal increase in kinetic losses at the cathode and the anode, and energy loss from the production of unwanted hydrogen (i.e. reduced CO selectivity at high current densities). These results suggest that research and development efforts focused on maintaining high product selectivities and low cell voltages at high current densities could be most beneficial to reduce costs of electrochemical CO_2 conversion to CO. In addition, developing lower-cost anion exchange membranes and replacing precious anode catalysts with abundant metal catalysts (such as Ni or Zn) are critical challenges. Unsurprisingly, our analysis showed that the viability of electrosynthesis of CO against natural gas reforming processes is contingent on the availability of low-cost, zero, or low-carbon electricity. Overall, these results support that CO_2 electrolysis is a developing technology with huge potential to create useful chemicals and fuels from waste CO_2 in near future. However, substantial efforts are required to overcome the current challenges.

Acknowledgements

This research received funding from the HBIS Group, China through the HBIS-UQ Innovation Centre for Sustainable Steel (ICSS) and Australian Research Council (ARC) Linkage Project LP160101729. S. Garg, Y. Wu, and M. N. Idros acknowledge scholarship support from the University of Queensland (UQ) Graduate School.

References

1. E. S. Rubin, J. E. Davison and H. J. Herzog, *International Journal of Greenhouse Gas Control*, 2015, **40**, 378-400.
2. Y. J. Sa, C. W. Lee, S. Y. Lee, J. Na, U. Lee and Y. J. Hwang, *Chemical Society Reviews*, 2020, **49**, 6632-6665.
3. D. M. Weekes, D. A. Salvatore, A. Reyes, A. Huang and C. P. Berlinguette, *Accounts of chemical research*, 2018, **51**, 910-918.
4. Z. D. Dong, L. J. Long and Q. S. Zhang, *Advanced Materials*, 2016, **28**, 3423-3452.
5. D. A. Salvatore, C. M. Gabardo, A. Reyes, C. P. O'Brien, S. Holdcroft, P. Pintauro, B. Bahar, M. Hickner, C. Bae, D. Sinton, E. H. Sargent and C. P. Berlinguette, *Nature Energy*, 2021, DOI: 10.1038/s41560-020-00761-x.
6. M. Jouny, W. Luc and F. Jiao, *Industrial & Engineering Chemistry Research*, 2018, **57**, 2165-2177.
7. J. Spurgeon and B. Kumar, *Energy & Environmental Science*, 2018, DOI: 10.1039/C8EE00097B.
8. S. Verma, B. Kim, H.-R. M. Jhong, S. Ma and P. J. A. Kenis, *ChemSusChem*, 2016, **9**, 1972-1979.
9. P. De Luna, C. Hahn, D. Higgins, S. A. Jaffer, T. F. Jaramillo and E. H. Sargent, *Science*, 2019, **364**, eaav3506.
10. R. I. Masel, Z. Liu, H. Yang, J. J. Kaczur, D. Carrillo, S. Ren, D. Salvatore and C. P. Berlinguette, *Nature Nanotechnology*, 2021, DOI: 10.1038/s41565-020-00823-x.
11. R. B. Kutz, Q. Chen, H. Yang, S. D. Sajjad, Z. Liu and I. R. Masel, *Energy Technology*, 2017, **5**, 929-936.
12. M. Carmo, D. L. Fritz, J. Mergel and D. Stolten, *International Journal of Hydrogen Energy*, 2013, **38**, 4901-4934.
13. F. Lu, M. Zhou, Y. Zhou and X. Zeng, *Small*, 2017, **13**, 1701931.
14. T. Zhang, Y. Zhu and J. Y. Lee, *Journal of Materials Chemistry A*, 2018, **6**, 8147-8158.
15. Battelle, *Manufacturing cost analysis of 10 kw and 25 kw direct hydrogen polymer electrolyte membrane (pem) fuel cell for material handling applications*, Report DE-EE0005250, Battelle Memorial Institute, Columbus, OH, 2013.
16. Battelle, *Manufacturing Cost Analysis of 1, 5, 10 and 25 kW Polymer Electrolyte Membrane (PEM) Fuel Cell Systems for Material Handling Applications*, U.S. Department of Energy, Energy Efficiency & Renewable Energy, Fuel Cell Technologies Office, 2017.
17. G. O. Larrazábal, P. Strøm-Hansen, J. P. Heli, K. Zeiter, K. T. Therkildsen, I. Chorkendorff and B. Seger, *ACS Applied Materials & Interfaces*, 2019, **11**, 41281-41288.
18. B. Endrődi, E. Kecsenovity, A. Samu, F. Darvas, R. V. Jones, V. Török, A. Danyi and C. Janáky, *ACS Energy Letters*, 2019, **4**, 1770-1777.
19. C. Dong, C. Lian, S. Hu, Z. Deng, J. Gong, M. Li, H. Liu, M. Xing and J. Zhang, *Nature Communications*, 2018, **9**, 1252.
20. R. Reske, H. Mistry, F. Behafarid, B. Roldan Cuenya and P. Strasser, *Journal of the American Chemical Society*, 2014, **136**, 6978-6986.
21. D. Kopač, B. Likozar and M. Huš, *ACS Catalysis*, 2020, **10**, 4092-4102.
22. Y. C. Li, Z. Yan, J. Hitt, R. Wycisk, P. N. Pintauro and T. E. Mallouk, *Advanced Sustainable Systems*, 2018, **2**, 1700187.
23. M. Ma, E. L. Clark, K. T. Therkildsen, S. Dalsgaard, I. Chorkendorff and B. Seger, *Energy & Environmental Science*, 2020, **13**, 977-985.
24. M. Ma, S. Kim, I. Chorkendorff and B. Seger, *Chemical Science*, 2020, **11**, 8854-8861.
25. A. Pătru, T. Binninger, B. Pribyl and T. J. Schmidt, *Journal of The Electrochemical Society*, 2019, **166**, F34-F43.
26. T. Luo, S. Abdu and M. Wessling, *Journal of Membrane Science*, 2018, **555**, 429-454.
27. B. Cermenek, J. Ranninger and V. Hacker, in *Ethanol*, eds. A. Basile, A. Iulianelli, F. Dalena and T. N. Veziroğlu, Elsevier, 2019, DOI: https://doi.org/10.1016/B978-0-12-811458-2.00015-8, pp. 383-405.
28. W. G. Colella, B. D. James, J. M. Moton, G. Saur and T. Ramsden, Golden, Colorado, 2014.
29. J. C. Fornaciari, M. R. Gerhardt, J. Zhou, Y. N. Regmi, N. Danilovic, A. T. Bell and A. Z. Weber, *Journal of The Electrochemical Society*, 2020, **167**, 104508.
30. Z. Liu, H. Yang, R. Kutz and R. I. Masel, *Journal of The Electrochemical Society*, 2018, **165**, J3371-J3377.
31. D. A. Salvatore, D. M. Weekes, J. He, K. E. Dettelbach, Y. C. Li, T. E. Mallouk and C. P. Berlinguette, *ACS Energy Letters*, 2018, **3**, 149-154.

32. H. W. Shafaque, C. Lee, K. F. Fahy, J. K. Lee, J. M. LaManna, E. Baltic, D. S. Hussey, D. L. Jacobson and A. Bazylak, *ACS Applied Materials & Interfaces*, 2020, DOI: 10.1021/acsami.0c14832.
33. T. N. Nguyen and C.-T. Dinh, *Chemical Society Reviews*, 2020, **49**, 7488-7504.
34. E. Jeng and F. Jiao, *Reaction Chemistry & Engineering*, 2020, **5**, 1768-1775.
35. US Department of Energy, *Carbon Capture, Utilization, and Storage: Climate Change, Economic Competitiveness, and Energy Security*, 2016.
36. D. Peterson, J. Vickers and D. DeSantis, *Hydrogen Production Cost From PEM Electrolysis - 2019*, Department of Energy, USA, 2019.
37. A. Paturska, M. Repele and G. Bazbauers, *Energy Procedia*, 2015, **72**, 71-78.
38. F. Bauer, C. Hulteberg and D. T. Persson Tobias, *SGC rapport*, 2013, **270**, 83.
39. M. T. Ho, G. W. Allinson and D. E. Wiley, *Industrial & Engineering Chemistry Research*, 2008, **47**, 4883-4890.
40. M. T. Ho, A. Bustamante and D. E. Wiley, *International Journal of Greenhouse Gas Control*, 2013, **19**, 145-159.
41. R. Zhao, L. Liu, L. Zhao, S. Deng, S. Li, Y. Zhang and H. Li, *Journal of Cleaner Production*, 2019, **214**, 440-451.
42. H. Kim, J. Lee, S. Lee, I.-B. Lee, J.-h. Park and J. Han, *Energy*, 2015, **88**, 756-764.
43. Q. Lu and F. Jiao, *Nano Energy*, 2016, **29**, 439-456.
44. S. Verma, S. Lu and P. J. A. Kenis, *Nature Energy*, 2019, **4**, 466-474.
45. J. J. Kaczur, H. Yang, Z. Liu, S. D. Sajjad and R. I. Masel, *C—Journal of Carbon Research*, 2020, **6**, 33.
46. B. M. Institute, *Manufacturing Cost Analysis of 1, 5, 10 and 25 kW Polymer Electrolyte Membrane (PEM) Fuel Cell Systems for Material Handling Applications*, U.S. Department of Energy, Energy Efficiency & Renewable Energy, Fuel Cell Technologies Office, 2017.
47. Factory Price For Iridium Dioxide Nanopowder IrO_2 Nanoparticle, https://www.hwnanomaterial.com/factory-price-for-iridium-dioxide-nanopowder-iro2-nanoparticle_p983.html, (accessed 15/08/2020, 2020).
48. Factory Price Sell Nano Silver Powder with Ag Nanoparticles and Nanopowder Dispersion, https://www.alibaba.com/product-detail/Nano-Ag-Powder-Silver-Nanoparticles-Nanopowder_62422781136.html, (accessed 15/08/2020, 2020).
49. T. Burdyny and W. A. Smith, *Energy & Environmental Science*, 2019, **12**, 1442-1453.
50. D. Salvatore and C. P. Berlinguette, *ACS Energy Letters*, 2020, **5**, 215-220.
51. J. A. Rabinowitz and M. W. Kanan, *Nature Communications*, 2020, **11**, 5231.
52. L.-C. Weng, A. T. Bell and A. Z. Weber, *Energy & Environmental Science*, 2019, **12**, 1950-1968.
53. T. Kimura and Y. Yamazaki, *Electrochemistry*, 2011, **79**, 94-97.
54. T. H. Pham, A. Allushi, J. S. Olsson and P. Jannasch, *Polymer Chemistry*, 2020, **11**, 6953-6963.
55. J. R. Varcoe, P. Atanassov, D. R. Dekel, A. M. Herring, M. A. Hickner, P. A. Kohl, A. R. Kucernak, W. E. Mustain, K. Nijmeijer, K. Scott, T. Xu and L. Zhuang, *Energy & Environmental Science*, 2014, **7**, 3135-3191.
56. W. H. Lee, Y.-J. Ko, Y. Choi, S. Y. Lee, C. H. Choi, Y. J. Hwang, B. K. Min, P. Strasser and H.-S. Oh, *Nano Energy*, 2020, **76**, 105030.
57. U. O. Nwabara, E. R. Cofell, S. Verma, E. Negro and P. J. A. Kenis, *ChemSusChem*, 2020, **13**, 855-875.
58. S. A. Mahyoub, F. A. Qaraah, C. Chen, F. Zhang, S. Yan and Z. Cheng, *Sustainable Energy & Fuels*, 2020, **4**, 50-67.
59. J. Na, B. Seo, J. Kim, C. W. Lee, H. Lee, Y. J. Hwang, B. K. Min, D. K. Lee, H.-S. Oh and U. Lee, *Nature Communications*, 2019, **10**, 5193.
60. Á. Vass, B. Endrődi and C. Janáky, *Current Opinion in Electrochemistry*, 2021, **25**, 100621.
61. Y. Zhang, Z. Han, B. Dong, Y. Yu, A. Kong and Y. Shan, *Catalysis Communications*, 2016, **86**, 119-123.
62. G. Juodeikiene, D. Vidmantiene, L. Basinskiene, D. Cernauskas, E. Bartkiene and D. Cizeikiene, *Catalysis Today*, 2015, **239**, 11-16.
63. C. C. Dorris, E. Lu, S. Park and F. H. Toro, *High-purity oxygen production using mixed ionic-electronic conducting sorbents*, University of Pennsylvania, 2016.
64. L. Yang, W. Liu, Z. Zhang, X. Du, L. Dong and Y. Deng, *Journal of Power Sources*, 2019, **420**, 99-107.
65. F.-Y. Gao, R.-C. Bao, M.-R. Gao and S.-H. Yu, *Journal of Materials Chemistry A*, 2020, **8**, 15458-15478.
66. J. Song, C. Wei, Z.-F. Huang, C. Liu, L. Zeng, X. Wang and Z. J. Xu, *Chemical Society Reviews*, 2020, **49**, 2196-2214.
67. D. Henkensmeier, M. Najibah, C. Harms, J. Žitka, J. Hnát and K. Bouzek, *Journal of Electrochemical Energy Conversion and Storage*, 2020, **18**.

68. Z. Liu, S. D. Sajjad, Y. Gao, H. Yang, J. J. Kaczur and R. I. Masel, *International Journal of Hydrogen Energy*, 2017, **42**, 29661-29665.
69. W.-H. Lee, E. J. Park, J. Han, D. W. Shin, Y. S. Kim and C. Bae, *ACS Macro Letters*, 2017, **6**, 566-570.
70. H.-Y. Jeong, M. Balamurugan, V. S. K. Choutipalli, E.-s. Jeong, V. Subramanian, U. Sim and K. T. Nam, *Journal of Materials Chemistry A*, 2019, **7**, 10651-10661.
71. S. Ren, D. Joulié, D. Salvatore, K. Torbensen, M. Wang, M. Robert and C. P. Berlinguette, *Science*, 2019, **365**, 367-369.
72. C. M. Gabardo, C. P. O'Brien, J. P. Edwards, C. McCallum, Y. Xu, C.-T. Dinh, J. Li, E. H. Sargent and D. Sinton, *Joule*, 2019, **3**, 2777-2791.
73. H. Koshikawa, H. Murase, T. Hayashi, K. Nakajima, H. Mashiko, S. Shiraishi and Y. Tsuji, *ACS Catalysis*, 2020, **10**, 1886-1893.
74. J. Lee, J. Lim, C.-W. Roh, H. S. Whang and H. Lee, *Journal of CO2 Utilization*, 2019, **31**, 244-250.
75. B. Endrődi, E. Kecsenovity, A. Samu, T. Halmágyi, S. Rojas-Carbonell, L. Wang, Y. Yan and C. Janáky, *Energy & Environmental Science*, 2020, **13**, 4098-4105.
76. S. Garg, M. Li, A. Z. Weber, L. Ge, L. Li, V. Rudolph, G. Wang and T. E. Rufford, *Journal of Materials Chemistry A*, 2020, **8**, 1511-1544.
77. E. J. Dufek, T. E. Lister and M. E. McIlwain, *Journal of Applied Electrochemistry*, 2011, **41**, 623-631.
78. R. Küngas, *Journal of The Electrochemical Society*, 2020, **167**, 044508.
79. M. Ramdin, A. R. T. Morrison, M. de Groen, R. van Haperen, R. de Kler, L. J. P. van den Broeke, J. P. M. Trusler, W. de Jong and T. J. H. Vlugt, *Industrial & Engineering Chemistry Research*, 2019, **58**, 1834-1847.
80. A. Raksajati, M. T. Ho and D. E. Wiley, *Industrial & Engineering Chemistry Research*, 2013, **52**, 16887-16901.
81. B. W. Griscom, J. Adams, P. W. Ellis, R. A. Houghton, G. Lomax, D. A. Miteva, W. H. Schlesinger, D. Shoch, J. V. Siikamäki, P. Smith, P. Woodbury, C. Zganjar, A. Blackman, J. Campari, R. T. Conant, C. Delgado, P. Elias, T. Gopalakrishna, M. R. Hamsik, M. Herrero, J. Kiesecker, E. Landis, L. Laestadius, S. M. Leavitt, S. Minnemeyer, S. Polasky, P. Potapov, F. E. Putz, J. Sanderman, M. Silvius, E. Wollenberg and J. Fargione, *Proceedings of the National Academy of Sciences*, 2017, **114**, 11645-11650.
82. V. Vij, S. Sultan, A. M. Harzandi, A. Meena, J. N. Tiwari, W.-G. Lee, T. Yoon and K. S. Kim, *ACS Catalysis*, 2017, **7**, 7196-7225.
83. X. Hu, X. Tian, Y.-W. Lin and Z. Wang, *RSC Advances*, 2019, **9**, 31563-31571.
84. *Australia Pat.*, 2006.
85. N. M. Haegel, R. Margolis, T. Buonassisi, D. Feldman, A. Froitzheim, R. Garabedian, M. Green, S. Glunz, H.-M. Henning, B. Holder, I. Kaizuka, B. Kroposki, K. Matsubara, S. Niki, K. Sakurai, R. A. Schindler, W. Tumas, E. R. Weber, G. Wilson, M. Woodhouse and S. Kurtz, *Science*, 2017, **356**, 141-143.

Supplementary Information

Is maximising current density always the optimum electrolyser design strategy for electrochemical CO_2 conversion to chemicals?

Sahil Garg[a,1], Mengran Li [a,2,*], Mohamed Nazmi Idros [a], Yuming Wu [a], Geoff G.X. Wang [a], Thomas E. Rufford [a,*]

[a] *School of Chemical Engineering, the University of Queensland, St Lucia, 4072, Brisbane, Queensland, Australia*

[1] Present address for S. Garg: *Surface Physics and Catalysis (SurfCat) Section, Department of Physics, Technical University of Denmark, 2800 Kgs. Lyngby, Denmark*

[2] Present address for M. Li: *Materials for Energy Conversion and Storage (MECS), Department of Chemical Engineering, Faculty of Applied Sciences, Delft University of Technology, van der Maasweg 9, 2629 HZ Delft, The Netherlands*

**Corresponding authors: T.Rufford t.rufford@uq.edu.au; M. Li m.li6@uq.edu.au*

1 Experimental methods

1.1 Preparation of the silver gas diffusion electrode (GDE)

To prepare the Ag-GDE, 90 mg of Ag nanoparticles (20-40 nm, Alfa Aesar) were suspended in 0.3 mL Millipore water and 0.6 mL isopropyl alcohol (IPA, ≥ 99.7%, Sigma Aldrich). The resulting suspension was sonicated for 15 min to ensure uniformity. After sonication, the catalyst ink was used to spray coat a gas diffusion layer (GDL 240, FuelCell Store) to achieve a loading of 2.0 ± 0.1 mg·cm^{-2}.

1.2 CO_2 electrolyser assembly and operation

We used a custom-built vapor-fed CO_2 electrolyser for performing CO_2R experiments. The main components of the CO_2 electrolyser involve an Ag-GDE as a cathode, IrO_2-based GDE as an anode (Dioxide Materials), cathode and anode serpentine flow fields (made of titanium), an anion-exchange membrane (AEM Sustainion®, X37-50 grade, Dioxide Materials). The active geometric area of the cathode was 5 cm^2 while the anode had an active area of 9 cm^2. The anode and cathode were separated by an AEM. The catalyst sides of the anode and cathode

each faced towards the AEM (**Figure S1**). Silicon gaskets were used between each layer to ensure proper liquid and gas sealing. After electrolyzer assembly, humidified CO_2 (23 ± 2 ˚C) was supplied to the cathode side at a constant flow rate of 60 sccm via the mass flow controller (pMFC, MKS instruments, ± 1% precision), while a 10 mM $KHCO_3$ (anolyte, ≥ 99.5% Sigma Aldrich) was circulated in the anode flow field at a constant flow rate of 1 mL·min^{-1}. Also, we used a stack consisting of two cells (with a total active cathode area of 10 cm^2) connected with a titanium bipolar plate engraved with serpentine flow fields on both sides.

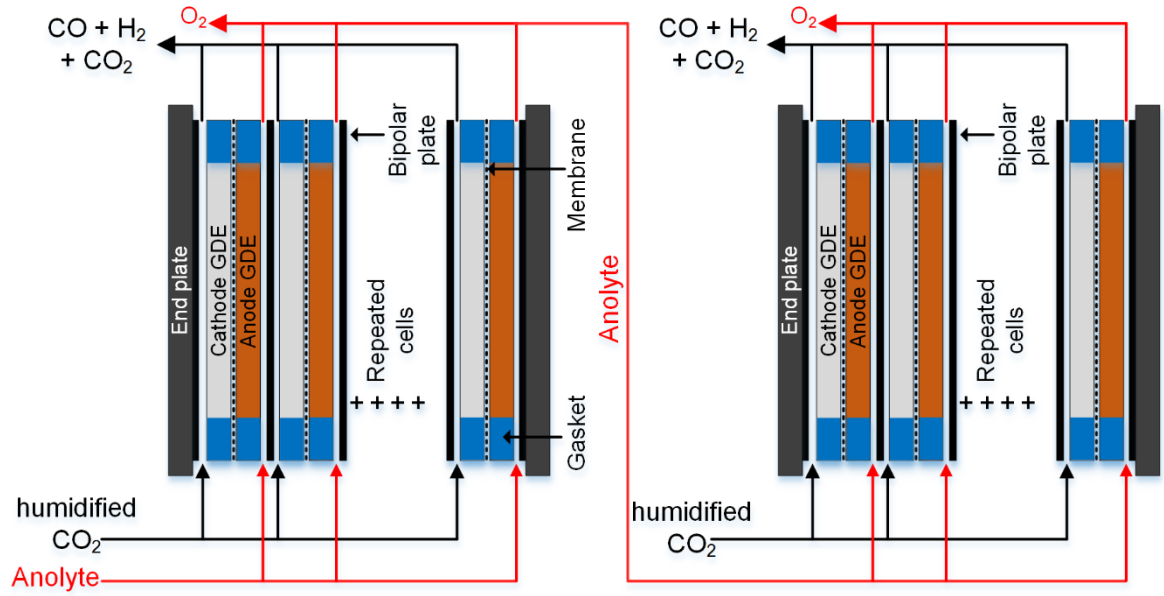

Figure S1. Schematic of the vapor-fed cell showing how CO_2 and electrolyte flow take place in the electrolyser stack used in this study for the analysis.

The electrochemical CO_2 experiments were performed at constant current density (galvanostatic-mode) using a potentiostat (Autolab PGSTAT302N) in a two-electrode configuration. The effluent gases (unreacted CO_2 + CO + H_2) from the electrolyser were analyzed using an inline gas chromatograph (GC 2030, Shimadzu) equipped with both the thermal conductivity and flame ionization detector. A digital flowmeter (Optiflow 520, Sigma-Aldrich) was used to measure the flow rate of the effluent gases. After the electrolyser is set on the constant current operation, the potential was stabilized for at least 500 s before the GC analysis was performed. For accurate measurement of electrochemical results, the cell voltage was averaged over a 100 s time interval; and three separate gas injections were analyzed at regular intervals and a mean value was reported. All cell voltages reported are actual measured values without any *iR* correction.

The faradaic efficiency (FE) for CO production was calculated using the following equation:

$$FE(\%) = \frac{znF}{Q} \times 100 \qquad \text{(S1)}$$

The partial current density was then calculated by multiplying the faradaic efficiency with the total current density. For the long-term stability tests, a constant current density of 1000 $A \cdot m^{-2}$ was applied across the electrolyser stack. The anolyte (10 mM $KHCO_3$) was changed every 24 hours during this test to maintain the concentrations and conductivity of the ions in the anolyte flow-field. The cell potential was monitored and the FE was calculated every 2 hours.

We used experimental CO_2R results to describe the relationship between cell voltage (E_{cell}) and current density (j) using a polarization model (Equation S2) that involves thermodynamic cell voltage (E_o), kinetic overpotential (η_{kin}), mass transport overpotential (η_{mt}), and ohmic losses (j x ASR). ASR represents the area-specific resistance of the Sustainion® AEM. Butler-Volmer (B-V) (Equation S3) kinetic theory can be used to describe the kinetic overpotential, where j_o is the exchange current density, α is the charge transfer coefficient, z is the number of electrons required to produce one mole of CO (i.e. 2), R is the universal gas constant, and T is the absolute temperature (assumed ambient temperature = 298 K for both anodic and cathodic reactions). The B-V equation is only valid for small overpotentials, however, we observed large overpotentials in experimental CO_2R data, therefore, we used the Tafel equation (Equation S4) to estimate the kinetic overpotential (η_{kin}), where A represents the Tafel slope. We took 0.1 $A \cdot m^{-2}$ as the value of j_o with the assumption that both the cathode and anode have a very high active surface area. To understand the behavior of j_o on the estimation of kinetic overpotential, we did a sensitivity analysis by changing the values of j_o and observe that varying j_o does not affect the kinetic overpotential significantly (**Figure S2A**). The values of kinetic overpotentials at different current densities were then calculated by fitting the Tafel slope (A) in Equation S4. We also calculated kinetic overpotential using the B-V equation (**Figure S2B**) by assuming a low charge transfer coefficient (α) of 0.1 for the high Tafel slope. We did not observe any significant difference in the kinetic overpotential data estimated from the Tafel slope and B-V equation.

$$E = E_o + \eta_{kin} + \eta_{mt} + j \times ASR \qquad \text{(S2)}$$

$$j = j_o \left(\exp\left(-\frac{\alpha \eta_{kin} zF}{RT} \right) - \exp\left(\frac{(1-\alpha)\eta_{kin} zF}{RT} \right) \right) \qquad \text{(S3)}$$

$$\eta_{kin} = A * Log_{10}\left(\frac{j}{j_o}\right) \quad \text{(S4)}$$

$$\eta_{mt} = \frac{RT}{zF}\ln\left(1-\frac{j}{j_{\lim}}\right),\ j_{\lim} = -\frac{zFDC_f(1-X)}{\delta} \quad \text{(S5)}$$

$$E_o = E^{\theta} + \frac{RT}{zF}\ln\left(\frac{1-X}{X \cdot FE_{CO}}\right) \quad \text{(S6)}$$

Although the GDE used in our experiments is not planar, we modeled the limiting current density (j_{lim}) in the electrolyser using a linear diffusion profile to the planar electrode, where j_{lim} is defined as the current density at which the CO_2 concentration near the electrode surface is close to zero. Both the limiting current density and mass transport overpotential were calculated by Equation S5, where D is the molecular diffusion coefficient (2.2 x 10^{-9} $m^2 \cdot s^{-1}$)[1] across a boundary-layer thickness (δ = 3 x 10^{-6} m)[2] in a planar electrode, X is the single-pass conversion, and C_f is the concentration of CO_2 in the feed to the electrolyser. Before these overpotentials can be combined into the thermodynamic cell voltage (E_o) to calculate the overall cell voltage (Equation S2), the change in standard conditions to the actual operating conditions must be considered using the Nernst Equation S6,[2] where E^{θ} is the difference of the standard reduction potentials of the anodic and cathodic half-cell reactions. For more details on Equations S2 to S6, we refer the readers to the general TEA paper by Brushett and co-workers.[2] Now that all the overpotentials can be computed, we can use equation S2 to calculate how the breakdown of the overall cell voltage of the electrolyser behaves at different CDs.

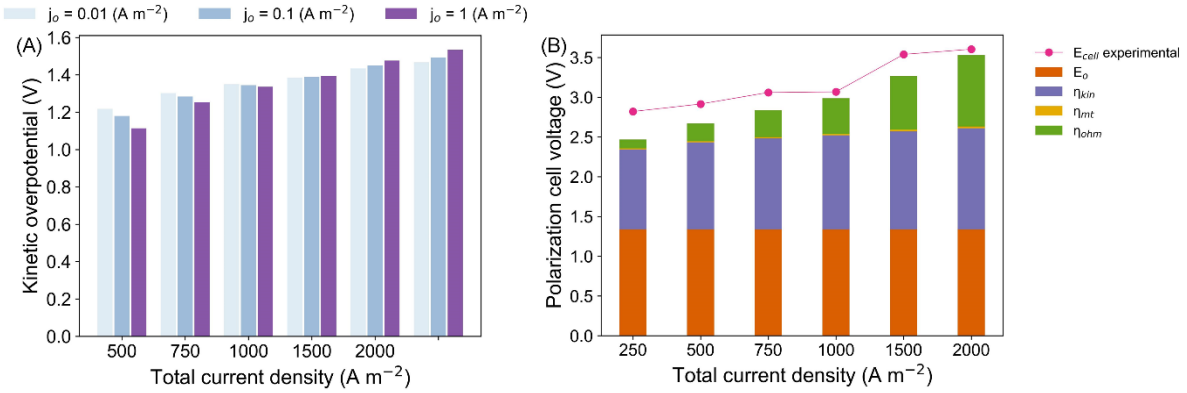

Figure S2. (A) Change in kinetic overpotential (estimated from Equation S4) when the exchange current density (jo) was varied between 0.01 to 1 A·m^{-2}; (B) Polarization results showing the cumulative voltage breakdown including the thermodynamic voltage, kinetic overpotential, mass transport overpotential, and ohmic losses. Where kinetic overpotential was calculated from Equation S3, and exchange current density (j_o) and charge transfer coefficient were assumed to be 0.1 A·m^{-2} and 0.1 respectively.

2 Methodology for CO_2R process in the TEA study

2.1 Process model description

A general process flow sheet for electrochemical conversion of CO_2R to CO is presented in **Figure S3** with three major units: (1) capture of CO_2 from industrial sources to provide enriched CO_2 to the electrolyser; (2) the electrolyser; and (3) a gas separation unit to recover CO and H_2 from unreacted CO_2, which can be recycled to the electrolyser.

There exist many technologies for CO_2 capture from industrial waste gases and flue gases, including absorption, adsorption, or cryogenic separation.[3-5] Among these, amine-based absorption is the most suitable technology for capturing CO_2 from high volume flue gas streams and providing a high purity (> 99%) CO_2 product.[6] For my TEA, we assumed the cost of CO_2 capture by aqueous monoethanolamine (MEA) to be 60$ per ton CO_2 captured.[7] Further, we assumed that the CO_2 coming out of the stripper (operating at 1.5 bar and 120˚C) of the acid-gas removal system was saturated with water (calculated from Aspen Plus) and did not have any MEA vapors.

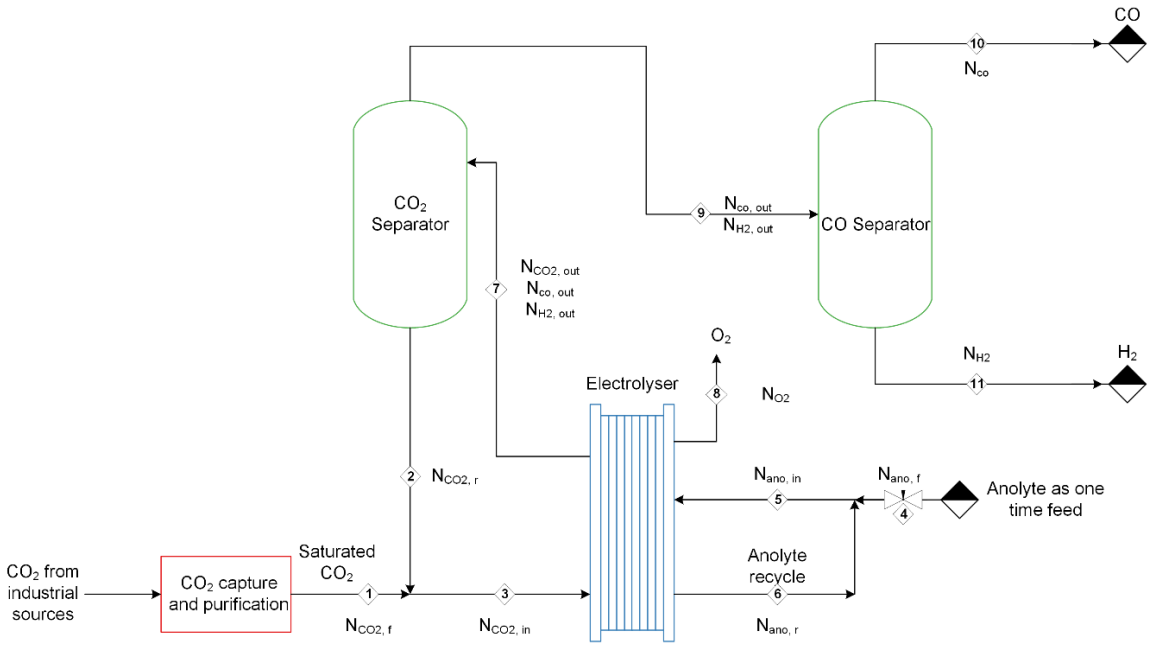

Figure S3. A process flow diagram for electrochemical reduction of CO_2 to CO.

Next, the saturated CO_2 is fed to the CO_2 electrolyser at the cathode side while the 10 mM $KHCO_3$ as anolyte was supplied to the anode side. The following reactions occur at the cathode and anode during CO_2R:

At the cathode:

$$CO_2 + H_2O + 2e^- \rightarrow CO + 2OH^- \quad \text{(S7)}$$

$$CO_2 + H_2O + 2e^- \rightarrow HCOO^- + OH^- \quad \text{(S8)}$$

$$2H_2O + 2e^- \rightarrow H_2 + 2OH^- \quad \text{(S9)}$$

$$CO_2 + OH^- \rightarrow HCO_3^- \quad \text{(S10)}$$

$$HCO_3^- + OH^- \rightarrow CO_3^{2-} \quad \text{(S11)}$$

At the anode:

$$2OH^- \rightarrow \frac{1}{2}O_2 + H_2O + 2e^- \quad \text{(S12)}$$

$$OH^- + H^+ \rightarrow H_2O \quad \text{(S13)}$$

$$HCOO^- \rightarrow CO_2 + H^+ + 2e^- \quad \text{(S14)}$$

$$HCO_3^- + H^+ \rightarrow CO_2 + H_2O \quad \text{(S15)}$$

$$CO_3^{2-} + 2H^+ \rightarrow CO_2 + H_2O \quad \text{(S16)}$$

Reaction S7 shows that one mole of CO_2 consumed at the cathode produces 2 moles of hydroxide ions that are transported across the AEM and oxidized at the anode (Reaction S12), meaning there is no net consumption of water. In the case of HER (Reaction S9), 2 moles of water produces one mole of H_2 and 2 moles of hydroxide which only then form one mole of water at the anode. Therefore, during HER, every one mole of H_2 produced at the cathode consumes one mole of water from the saturated CO_2. Further, Reactions S10 and S11 show the production of bicarbonate and carbonate ions. These ions could be transferred to the anode side across the AEM, and at the anode be oxidized back into CO_2 (Reactions S15 and S16). However, we assumed that there are no losses and transportation of CO_2 from the cathode to the anode side.

From the CO_2 electrolyser, CO is produced in the gaseous form, so we assume that pressure swing adsorption (PSA) is suitable to separate the CO from H_2 (side-product) and unreacted CO_2, which has been demonstrated to achieve over 99% efficiency.[8] Unreacted CO_2 is recycled back to the electrolyser and H_2 is separated from the CO.

2.2 **CO_2 electrolyser and stack operation**

The key assumptions used in our model of the CO_2 electrolyser were:

- The whole CO_2 electrolyser stack including each cell operates at constant and ambient pressure and temperature.
- The CO_2 electrolyser and gas separation unit run on electricity from a zero-carbon emissions source.
- Each cell in the stack operates at steady-state and has a uniform production rate (constant current density and voltage) during its lifetime in such a way that it is not sensitive to change in concentration of anolyte.
- CO_2 mass transport at the cathode is unidirectional and diffusion is perpendicular to the CO_2 flow.
- The AEM operates stably without any reactants or products crossover between the anode and cathode chambers throughout its lifetime and has an area-specific resistance of 0.00045 $\Omega \cdot m^2$ (Dioxide Materials).
- The catalyst loading is 2 mg cm^{-2} on the cathode (Ag-GDE) and 1 mg cm^{-2} on the anode (IrO_2-GDE).
- A single-pass CO_2 conversion of 50% in each cell is achieved.[9]
- The conductivity of anolyte remains constant over CO_2 electrolysis time within different stacks.
- According to common industry practices, the cells are rectangular in geometry and arranged hydraulically in parallel and electrically in series within the stack, whereas the stacks are arranged in parallel.[10]
- To calculate the necessary catalyst area and voltage requirement, each stack operates at a constant current density.
- We assumed that the protons required for the HER originate in the water in the CO_2 feed.
- At the anode, a one-time anolyte feed is provided to the electrolyser which is recycled back and no loss of anolyte is assumed.

To solve the fundamental mass and energy balance equations, we used a process flow sheet shown in **Figure S3**. As per mass-balance for the product across the cathode chamber, no product is introduced into the reactor and the amount of product formed can be calculated from Faraday's law, current density (j), and active cathode area (A). So assuming steady-state

conditions (no change in concentration of product with time), Equation S17 can be used to calculate the $\dot{N}_{CO,out}$:

$$0 = \dot{N}_{CO,out} + \frac{FE_{CO}\, jA}{z_{CO} F} \tag{S17}$$

where FE_{CO} is the faradaic efficiency of CO, z_{CO} is the number of electrons required to make one mole of CO (i.e. 2), and F is the Faraday's constant.

Since protons for HER comes from the saturated CO_2 (captured) stream, therefore, hydrogen production rate ($\dot{N}_{H_2,out}$ as a side/competing product) can be calculated by performing mass-balance for H_2 across the cathode chamber using Equation S18 as follows:

$$0 = \dot{N}_{H_2,out} + \frac{FE_{H_2}\, jA}{z_{H_2} F} \tag{S18}$$

where FE_{H_2} is the faradaic efficiency of H_2 and z_{H_2} is the number of electrons required to make one mole of hydrogen (i.e. 2).

If we define a single-pass conversion (X) of CO_2 across the electrolyser, then we can calculate the exit reactant flow-rate ($\dot{N}_{CO_2,out}$) as:

$$\dot{N}_{CO_2,out} = \dot{N}_{CO_2,in}(1 - X) \tag{S19}$$

Based on the mass-balance of the CO_2 across the cathode chamber, we can determine the amount of reactant being fed ($\dot{N}_{CO_2,in}$) to the electrolyser by substituting Equations S17 and S19 as:

$$\dot{N}_{CO_2,in} = \dot{N}_{CO_2,out} + \dot{N}_{CO,out} = -\frac{jAFE_{CO}}{XFz_{CO}} \tag{S20}$$

Assuming a 100% separation efficiency of gas-separators (**Figure S3**), a mass-balance across the separation unit provides the following equations:

$$\dot{N}_{CO_2,r} = \dot{N}_{CO_2,out} \tag{S21}$$

$$\dot{N}_{CO} = \dot{N}_{CO,out} \tag{S22}$$

$$\dot{N}_{H_2} = \dot{N}_{H_2,out} \tag{S23}$$

Since we are controlling the amount of fresh CO_2 that is being reduced ($\dot{N}_{CO_2,f}$), substituting Equations S20 and S21 into the mass-balance equation across the CO_2 recycle stream provides the amount of total CO_2 being fed ($\dot{N}_{CO_2,in}$) to the electrolyser:

$$\dot{N}_{CO_2,in} = \dot{N}_{CO_2,f} + \dot{N}_{CO_2,r} = \frac{\dot{N}_{CO_2,f}}{X} \tag{S24}$$

Now we can calculate the required cathode area (A) for treating $\dot{N}_{CO_2,in}$ using Equations S20 and S24 as:

$$A = \frac{XFz_{CO}\,\dot{N}_{CO_2,f}}{jFE_{CO}\left\{1-\phi_s\cdot(1-X)\right\}} \tag{S25}$$

The above equation can be used to calculate the amount of H_2 being produced by substituting Equation S25 into equation S17. At the cathode side, every one mole of H_2 formed consumes one mole of water. Therefore, to calculate the amount of water consumed or make-water required ($\dot{N}_{H_2O,make-up}$) in the saturated CO_2 stream, we used the following equation:

$$\dot{N}_{H_2O,make-up} = \dot{N}_{H_2,out} \tag{S26}$$

To calculate the power requirements of the whole CO_2 electrolyser plant, we need to determine the voltage needed to run the electrolyser at the desired current density. Generally, researchers used a fixed value of voltage[11, 12] in their model, and perform a sensitivity analysis, however, it is mostly proportional to the current flowing through the cell. So, if we increase the current density of the electrolyser, the required voltage should increase which was not considered in the previous studies.[11, 12] The overall voltage (E) across the electrolyser can be calculated by the following equation:

$$E = E_o + \eta \tag{S27}$$

Where E_o is the thermodynamic cell voltage and η is the overpotential arising from kinetics, mass-transfer, and ohmic losses. In my TEA model, we used the linear relationships between the CD (j) and cell voltage (E), and CD (j) and faradaic efficiency (FE) based on the experimental data as mentioned in section 2 of the main manuscript. The overall electrolyser voltage can be used to determine the power (P) requirement of the overall plant as

$$P = E\cdot jA \tag{S28}$$

2.3 **Economics of the CO_2 electrolyser**

To determine the economic feasibility, we used a simple cost metric, namely, the levelized cost of the CO production (C), as shown in the following equation:

$$C\ (\$\cdot kg\ CO_{prod.}^{-1}) = \frac{C_{op} + \frac{C_{capital,\ stack} + C_{BOP}}{t_y}}{\dot{N}_{CO} * M_{CO} * t_d} \quad \text{(S29)}$$

where C_{op} is the operating cost (per year) of the electrolyser; $C_{capital,\ stack}$ is the capital cost of the stack (including endplates, bipolar plates, gaskets, stack assembly, stack testing and conditioning, membrane, and cathode and anode catalyst costs); C_{BOP} is the balance of plant cost; $\dot{N}_{CO}$ is the outlet molar flow rate of CO from the electrolyser (mol/s); M_{CO} is the molecular weight of the CO (kg·mole^{-1}); t_y is the plant lifetime (20 years); t_d is the plant operating time in a year (340 days·year^{-1}). The economic feasibility can thus be determined by comparing the levelized Cost of the CO production to the present market price of the CO (i.e. 0.60 \$·kg^{-1}).[13]

The details of the design parameters for the components of the CO_2 electrolyser stack are shown in **Table S1**. The capital cost estimation factors of different components of the CO_2 electrolyser stack were adapted from the US Department of Energy's (DOE's) H2A analysis report for alkali water electrolyser (2017)[14] and listed in **Table S2**. These cost factors were estimated from the data provided to run a 25 kW fuel cell system equipped with 1000 stacks. Although increasing the number of stacks to more than 1000 may decrease the cost per stack, we did not consider any variation in cost with the change in the number of stacks required in my model. The balance of plant (BoP) cost including CO_2 delivery system, water/electrolyte delivery system, O_2 management system at the anode, thermal management, power electronics, control and sensors, the mechanical balance of plant, and item breakdown – assembly labor, etc. were assumed to be 53% of the total CO_2 electrolyser capital cost based on H2A analysis report.[14-16] The basis for economic calculations were based on treating 50 tons of CO_2 daily with a 20-year plant lifetime. Three weeks each year of downtime for plant maintenance was considered.

Table S1. Details of design parameters of each CO_2 electrolyser stack.[14, 17, 18]

Parameter	Value	Units
No of cells in one stack (N_{cell})	20	-
Active electrode area per cell (A_{elec})	0.04	m^2
Cathode catalysts loading (Cat_{load})	0.02	kg/m^2
Anode catalyst loading (Ano_{load})	0.01	kg/m^2
Thickness of the endplate (th_{ep})	0.006	m
Thickness of the bipolar plate (th_{bp})	0.004	m

Table S2. Estimation of the capital cost for the components of the CO_2 electrolyser stack including details of the material cost. The value of factors mentioned in the table is adapted from the US Department of Energy (DOE) H2A analysis report for a 25 kW system with 1000 units.[14]

Component	Material Cost ($/component)	Cost factor (finished product to the material)	Count per stack
End plate	1.26	6.19	2
Bipolar plate	0.71	4.10	21
Gasket	0.65	1.75	90
Membrane electrode assembly	8.62	2.16	20
Cathode catalyst (Ag for CO)	0.44	1	20
Anode catalyst (IrO_2)	0.32	1	20
Stack assembly	127.96	1	1
Stack testing and conditioning	127.30	1	1

The annual operating cost is the sum of the cost of CO_2 feed to the electrolyser, power requirements to reduce the CO_2 into CO, stack replacement (including cathode and anode), and water consumption at the anode. The stack was assumed to be replaced every 7 years and the replacement cost was estimated to be 15% of the total capital cost of the electrolyser unit.[19]

2.3.1 Electrolyser's capital cost

Based on the comprehensive costing analysis, the total installed capital cost (excluding BOP) was estimated to be around 4201 $\$\cdot m^{-2}$ of the cathode area. The total installed capital cost we calculated here shows a difference with the numbers reported in the literature.[2, 11, 12] The difference in total installed capital cost can be attributed to the use of different costing analysis; a more detailed analysis in this work as compared to the fixed installed capital cost in the literature. For example, Spurgeon and Kumar[12] used 16,280 $\$\cdot m^{-2}$, Brushett and co-workers[2] employed 11,700 $\$\cdot m^{-2}$, while Jiao's group[11] assumed 920 $\$\cdot m^{-2}$ as the total installed capital cost. Both Spurgeon and Brushett's groups extracted the installed capital cost ($\$\cdot m^{-2}$) from different H2A case studies where power density to produce hydrogen from PEM electrolysers (38 $kW\cdot m^{-2}$, that operate at low voltage and high current density)[20] are much higher as compared to the CO_2 electrolysers (3.17 $kW\cdot m^{-2}$, that operate at high voltage and low current density). Whereas, Jiao's group[11] extracted the same numbers from a 2007 H2A report where the electrolyser ran on a power density of 3.06 $kW\cdot m^{-2}$. And since the power density of PEM

electrolyser (3.06 $kW \cdot m^{-2}$) used by the Jiao's group is similar to this work (3.17 $kW \cdot m^{-2}$) and therefore we observed relatively smaller variations in the total installed capital cost with the Jiao's group as compared to the other two groups.

2.3.2 Cost of membrane

We used a Sustainion anion exchange membrane (AEM) from Dioxide Materials in the CO_2 electrolyser. The price of the AEM is 221 $ for a piece of 23 cm x 28 cm which is equivalent to 3431.68$/$m^2$. However, the cost of material generally decreases with increasing purchase volume, therefore, we used a learning curve analysis[21, 22] to estimate the price of Sustainion AEM when purchasing large volumes for the techno-economic model.

The equation for a general learning curve is:

$$Y = AX^{b} \tag{S30}$$

where Y the new price of the AEM when purchasing in large quantity (50,000 units); A is the original price of Sustainion AEM (3432 $/$m^2$); X is the number of units (we assumed it to 50,000); b = log(m)/log(2) and m is the slope of the learning curve. The value of m (0.86) was taken from the H2A analysis report.[21] From equation (S30), we calculated the new price of AEM to be 325$/$m^2$.

2.3.3 Cost of gas separation

For gas separation, generally, three different techniques such as amine scrubbing, physical scrubbing, and pressure swing adsorption (PSA) are utilized. Among them, PSA is the commercially used techniques with lower capital and operating costs, and higher efficiency.[8] From the CO_2 electrolyser, the exit gas streams consist of unreacted CO_2, CO, and H_2. The gas separation required in this process is similar to the upgrading of biogas which typically contains an equimolar mixture of CO_2 and biomethane.[8] Based on the literature studies on PSA,[8, 11, 23] a reference capital cost of US$ 1,990,000 per 1000 m^3/h and an operating cost comprising of electricity only at 0.25 kWh/m^3 with a scaling exponent of 0.8 and a 100% CO_2 recycling efficiency were taken in this study. The transportation and compression costs of the purified gases were not taken into account in this study. We used the following equation to calculate the capital cost of PSA required in our analysis.

$$I_P = I_R * \left(\frac{Q_P}{Q_R} \right)^{b} \tag{S31}$$

where I_P is the capital cost of the proposed PSA, I_R is the capital cost of the reference PSA plant (1,990,000 $), Q_P is the capacity of the proposed PSA, Q_R is the capacity of the reference PSA, and b is the scaling factor.

In addition to PSA, we also used the Sherwood plot[24] approach to determine the CO separation cost. Dahmus and Gutowski[24] proposed a refined model of the Sherwood plot where the separation cost of three different categories of materials can be connected using the following equation.

$$P_{sep} = \frac{k_p}{C_i} \tag{S32}$$

where P_{sep} is the price of a product of interest that has a concentration of C_i in an initial mixture, and k_p is the separation factor in $\$\cdot kg^{-1}$ to process the total mixture. Based on the study conducted by Dahmus and Gutowski[24], k_p for gas separation was taken as 0.001 $\$\cdot kg_{mixture}^{-1}$. It is important to note that the exclusive capital cost for separation processes is not presented in our analysis, however, the gas separation cost includes profit margin, capital, and operational costs.

Table S3. Range of the parameters for the sensitivity analysis.

Operating parameters	Low values	Base values	High values
Single pass conversion (%)	-50%	50	+50%
Cell parameters			
Stack replacement interval (year)	4	7	10
Stack replacement cost (% of installed capital cost)	-50%	15	+50%
Economic parameters			
Price of the cathode (($\cdot kg^{-1}$)	-50%	800	+50%
Price of the anode (($\cdot kg^{-1}$)	-50%	120000	+50%
Price of feed CO_2 ($\cdot ton^{-1}$ CO_2 captured)	-50%	60	+50%
Price of electricity ($\cdot kWh^{-1}$)	-50%	0.06	+50%
Price of the membrane ($\cdot m^{-2}$)	-50%	325	+50%

3 References

1. M. J. W. Frank, J. A. M. Kuipers and W. P. M. van Swaaij, *Journal of Chemical & Engineering Data*, 1996, **41**, 297-302.
2. M. J. Orella, S. M. Brown, M. E. Leonard, Y. Román-Leshkov and F. R. Brushett, *Energy Technology*, 2020, **8**, 1900994.
3. A. Ali, K. Maqsood, L. P. Shin, V. Sellappah, S. Garg, A. B. M. Shariff and S. Ganguly, *Journal of Cleaner Production*, 2018, **171**, 795-810.
4. A. B. Rao and E. S. Rubin, *Environ. Sci. Technol.*, 2002, **36**, 4467-4475.
5. M. T. Ho, A. Bustamante and D. E. Wiley, *International Journal of Greenhouse Gas Control*, 2013, **19**, 145-159.
6. J.-Y. Lee, T. C. Keener and Y. J. Yang, *J. Air Waste Manage. Assoc.*, 2009, **59**, 725-732.
7. M. T. Ho, G. W. Allinson and D. E. Wiley, *Energy Procedia*, 2009, **1**, 763-770.
8. A. Paturska, M. Repele and G. Bazbauers, *Energy Procedia*, 2015, **72**, 71-78.
9. B. Endrődi, E. Kecsenovity, A. Samu, F. Darvas, R. V. Jones, V. Török, A. Danyi and C. Janáky, *ACS Energy Letters*, 2019, **4**, 1770-1777.
10. A. Ursúa, P. Sanchis and L. Marroyo, in *Renewable Hydrogen Technologies*, eds. L. M. Gandía, G. Arzamendi and P. M. Diéguez, Elsevier, Amsterdam, 2013, DOI: https://doi.org/10.1016/B978-0-444-56352-1.00014-3, pp. 333-360.
11. M. Jouny, W. Luc and F. Jiao, *Industrial & Engineering Chemistry Research*, 2018, **57**, 2165-2177.
12. J. M. Spurgeon and B. Kumar, *Energy Environ. Sci.*, 2018, **11**, 1536-1551.
13. Q. Lu and F. Jiao, *Nano Energy*, 2016, **29**, 439-456.
14. Battelle, *Manufacturing cost analysis of 10 kw and 25 kw direct hydrogen polymer electrolyte membrane (pem) fuel cell for material handling applications*, Report DE-EE0005250, Battelle Memorial Institute, Columbus, OH, 2013.
15. B. James, W. Colella, J. Moton, G. Saur and T. Ramsden, *PEM Electrolysis H2A Production Case Study Documentation*, National Renewable Energy Lab. (NREL), Golden, CO (United States), 2013.
16. W. G. Colella, B. James and J. M. Moton, *Strategic Analysis Inc*, 2014.
17. V. Sumit, K. Byoungsu, J. H. R. "Molly", M. Sichao and K. P. J. A., *ChemSusChem*, 2016, **9**, 1972-1979.
18. F. Goodridge and K. Scott, in *Electrochemical Process Engineering: A Guide to the Design of Electrolytic Plant*, Springer US, Boston, MA, 1995, DOI: 10.1007/978-1-4899-0224-5_5, pp. 177-244.
19. D. H. König, M. Freiberg, R.-U. Dietrich and A. Wörner, *Fuel*, 2015, **159**, 289-297.
20. D. Peterson, J. Vickers and D. DeSantis, *Hydrogen Production Cost From PEM Electrolysis - 2019*, Department of Energy, USA, 2019.
21. B. M. Institute, *Manufacturing Cost Analysis of 1, 5, 10 and 25 kW Polymer Electrolyte Membrane (PEM) Fuel Cell Systems for Material Handling Applications*, U.S. Department of Energy, Energy Efficiency & Renewable Energy, Fuel Cell Technologies Office, 2017.
22. M. G.K. and N. D.A., in *Cost Estimation*, 2015, DOI: https://doi.org/10.1002/9781118802342.ch10, pp. 180-203.
23. J. Spurgeon and B. Kumar, *Energy Environ. Sci.*, 2018, DOI: 10.1039/C8EE00097B.
24. J. B. Dahmus and T. G. Gutowski, *Environmental science & technology*, 2007, **41**, 7543-7550.